Transport theory for kinetic emission of secondary electrons from solids

J. Schou
Physics Department, Association Euratom—Risø National Laboratory, DK-4000 Roskilde, Denmark
(Received 26 December 1979)

Kinetic secondary electron emission from a solid target resulting from incidence of keV electrons or keV and MeV ions is treated theoretically on the basis of ionization cascade theory. The energy and angular distribution and the yield of secondary electrons are calculated for a random target. These quantities are determined from the solutions to a system of Boltzmann transport equations. Input quantities are the cross sections for collisions between the involved particles and the surface barrier of the target. A general power cross section has been utilized in the analytical procedure. It is shown that liberated electrons of low energy move isotropically inside the target in the limit of high primary energy as compared to the instantaneous energy of the liberated electrons. The connection between the spatial distribution of kinetic energy of the liberated electrons and the secondary electron current from a solid is derived. To find the former, existing computations for ion slowing down and experimental and theoretical ones for electron bombardment can be utilized. The energy and angular distribution of the secondary electrons and the secondary electron yield are both expressed as products of the deposited energy at the surface of the target and a factor which depends only on the properties of the escaping secondary electrons. Corrections for energy transport away from the surface by energetic recoil electrons are partly included. Also the contribution from recoiling target atoms at heavy-ion bombardment in the keV region is largely taken into account. The predicted energy and angular distribution agree with absolute spectra for incident electrons, whereas the agreement with absolute spectra for incident protons is less satisfactory. Extrapolation of the energy distribution down to the vacuum level gives a spectrum which shows good agreement with experimental data. The electron- and proton-induced yields from aluminum are evaluated on the basis of existing low-energy-electron stopping-power data. The agreement with existing experimental data is good. Also, experimental yields from electrons, protons, and noble gas ions incident on copper agree within the accuracy of the treatment.

I. INTRODUCTION

Irradiation of solids with charged or neutral particles is usually accompanied by emission of secondary electrons and of sputtered atoms or molecules.[1–5] In general the emission of electrons complicates all absolute beam current measurements in particle irradiation experiments, especially those where the current collected from a target is utilized for a determination of the beam current.[6,7] In fact, problems concerning secondary electron emission appear in studies of radiation effects in materials including plasma-surface interaction,[8–10] electron microscopy,[11] and related topics.[12]

Kinetic emission of secondary electrons from a solid is usually the result of a very large number of scattering and energy-loss processes[13,14]: incident *electrons* will generate secondary electrons by ionization of bound electrons or excitation of conduction electrons; these liberated electrons may undergo scattering by other electrons and target nuclei. For incident *ions with energy in the keV region or higher,* a cascade of recoiling target atoms may be generated. The primary ions and moving recoil atoms create excited electrons, which in turn may generate excited electrons. Some liberated electrons may be able to reach the surface of the solid; thus a certain fraction will escape and be registered as emitted secondary electrons. It is well known[15] that these emitted electrons originate mainly from a layer of the order of 5–20 Å below the surface in the case of metals and somewhat deeper in the case of semiconductors and insulators.

A qualitative picture of three cases of secondary electron emission is shown in Fig. 1. The random medium is bombarded by a primary electron, by a primary atom of the same kind as the target atoms, and finally by an arbitrary beam ion. The collisions between the particles under consideration in the present work will be described within the scheme of Bohr.[16] It means that the medium consists of a mixture of free electrons, i.e., electrons with velocities comparable to or less than the velocities of the primary particles, and of nuclei with strongly bound electrons. In the limit of very high primary velocities the medium can be viewed as consisting of bare nuclei and free electrons.

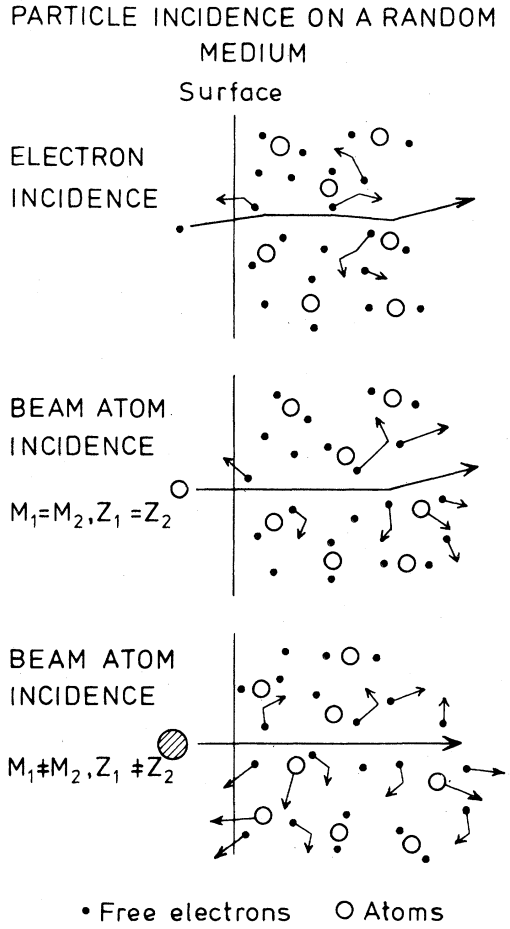

FIG. 1. Particle incidence on a random medium in three cases. The bombardment is assumed to cause emission of at least one secondary electron for all three particles. The density of moving particles is greatly exaggerated.

It is well known that the yield and energy spectrum of the secondary electrons is sensitive to the purity of the surface region of the solid.[1,3] Unfortunately, a considerable fraction of the existing data on secondary electron emission originates from experiments with poorly characterized surfaces. Thus, the development of ultra-high-vacuum equipment made possible a renewed activity in providing precise data for secondary electron emission from solids.

Apart from the kinetic emission of secondary electrons originating from the outermost bulk layers, the interaction of incident ions with solids may also lead to potential emission.[17] This is associated with the neutralization of the impinging ions before they reach the surface. The magnitude of this potential emission has been estimated by Kishinevsky.[18] Also, for the energies and ion-target combinations where potential emission may occur, the corresponding kinetic emission will to some extent be included in the present work. This requires some assumptions which will be discussed.

Electron-induced secondary electron emission[1,2,19,20] or ion-induced secondary electron emission[3–5,19] have been reviewed by several authors. However, only a few of these have studied both types of electron emission.

Baroody[21] formulated a theory for electron-induced secondary electron emission from metals. On the basis of a yield evaluation he pointed out that the existing data on the total secondary electron yield as a function of the primary energy could be scaled approximately to fall on a single curve. The velocity distribution of the emitted secondaries was also obtained by Baroody. However, some points in his work were later criticized by Hachenberg and Brauer.[2]

A large step forward toward a comprehensive theory was taken by Wolff,[13] who made a transport treatment for electron-induced secondary electron emission to obtain the spectrum of emitted secondaries, and to estimate the maximum yield. This treatment was later extended by Stolz.[22] Amelio[23] evaluated the energy distribution for the secondary electrons. All three authors concentrated on metals.

The absolute magnitude of the electron yield for ion energies well above the maximum of the electronic stopping power was evaluated by Sternglass.[14] For incident ions of low velocities Parilis and Kishinevsky[24,25] developed a theory which predicted the yield from metals on the basis of Auger recombination processes.

It is obvious, and implicitly contained in earlier work, that the secondary electron yield is related to the electronic stopping power,[1,13,14,24,26–32] or more precisely, the energy deposited into the electrons of the target. Since it has been demonstrated that the sputtering yield in a similar way is related to the energy deposited in motion of the target atoms,[33,34] there are striking similarities between fast-ion sputtering and secondary electron emission induced by fast particles. A more detailed discussion follows in Sec. II.

Experimental investigations of radiation damage, ion implantation, and sputtering have stimulated considerable progress in transport theory for energetic *atomic* particles.[35–37] Extensive tabulations[38,39] now exist of the distribution of energy deposited into damage or motion of the atoms, and the energy which ultimately is delivered to the target electrons.

The purpose of the present work has been to develop a theoretical treatment of the yield and energy distribution of secondary electrons from a random target. These electrons may originate either from keV or MeV ion and keV electron incidence. Because of the cascade nature of the processes leading to secondary electron emission it seems appropriate to utilize transport theoretical methods in studying

this emission. Furthermore, the successful application of transport methods for analyzing sputtering[33,40] has encouraged the use of similar methods in working with secondary electron emission.

The connection between secondary electron emission and the distribution of energy deposited into the electrons will be derived in the present work. The mentioned tabulations for atomic incidence will be largely utilized. However, the distribution of deposited energy for primary electrons as well turned out to be required for the evaluation of the secondary yield. The treatment is performed for liberated electrons inside the solid of energy sufficiently high that the detailed band structure is unimportant. The obtained secondary electron energy distribution may then be extrapolated down to the vacuum level. In most cases this extrapolation yields promising results; these are presented in Secs. IX and X.

The starting point is a Boltzmann-type transport equation. The input quantities are the cross sections for collisions between the interacting particles, the magnitude of the surface barrier, and possibly the binding energy of the liberated electrons. As these cross sections are not accurately known, extensive use will be made of model cross sections. The aim is to express the yields and the energy distributions by quantities that depend only weakly on the parameters specifying the model cross sections.

The basic equations for the distribution of liberated electrons in phase space are set up in Sec. II. The quantities necessary for the determination of the number of emitted secondary electrons, are governed by a system of equations which is treated in Secs. II and III. The applied cross sections for collisions between the involved particles are discussed in Sec. IV. The case of an incident electron is treated in Sec. V, while the relationship between the distribution of liberated electrons and the energy distribution is discussed in Secs. VI–VIII. The formulas for the energy and angular distribution of the emitted secondary electrons are obtained in Sec. IX, and the yield formulas are given in Sec. X. Finally, the role of recoiling target atoms in secondary electron emission and the distribution of energy, deposited by recoiling target atoms, are studied in Sec. XII.

Some results from this work have been presented recently.[41] Furthermore, the influence of recoiling target atoms has been treated in Ref. 42. In addition to the areas described above, the latter work includes a qualitative discussion of the relationship between the deposited energy and the secondary electron yield.

II. BASIC EQUATIONS

A. Theoretical starting point

This treatment is supposed to apply to both ion- and electron-induced secondary electron emission. The calculations assume in principle primary particles of high nonrelativistic energies; for ions this means energies at least in the keV region, whereas for primary electrons the energies may be somewhat lower. The treatment is applicable so long as a considerable fraction of the liberated low-energy electrons results from an ionization cascade. The calculations are performed for the specific case where the velocity of the incident particle is large compared to the velocities of the electrons which become liberated after interaction with the primary particle, and the velocities of the target atoms.

It is well known that the angular distribution of the secondaries ejected from noncrystalline solids is a cosine function both for ion[43] and electron incidence[44] at the energies considered here. This means that the angular distribution of the liberated electrons inside the solid must be roughly isotropic.[2] Furthermore, the ejected secondary electrons originate mainly at or just below a surface layer.[15] As sputtered particles display similar features[5,33,34] we shall make use of analogies with the theory of sputtering.[33,40]

Let us consider a random, monatomic medium. It is a convenient reference standard for understanding secondary electron emission. Furthermore, we assume a planar target surface. In the treatment here, as in similar multiple-collision problems, a semi-infinite target embedded in an infinite medium of the same material as the target is regarded a first step. As a second step one may introduce a real surface.

In the general treatment we do not specify whether our target is a metal, a semiconductor, or an insulator. Therefore, we just denote all excited internal secondaries as liberated electrons without regard to the target material. Obviously, the detailed band structure of the target material is important for the migration to and escape through the surface of the liberated low-energy electrons inside the solid.[1,2] However, as a starting point we shall, as mentioned in Sec. I, consider liberated electrons of energies (of the order 10–30 eV) somewhat above the Fermi energy or the bottom of the conduction band. The treatment in Sec. X concentrates on metals, but may also be extended to other materials.

The theoretical calculations do not include any effects of the charge of the beam ions. The difference between the yield from neutral, negative, or positive beam particles has apparently not been studied experimentally for the past ten years, and this subject will not be touched upon in the present work. Neither will the yield from molecular ions be analyzed.

Directional effects, which may occur in crystals, will not be treated in the present work.

Auger electrons are partly included in the treatment. The energy loss to the Auger processes is included in the stopping power; cascade electrons liberated by Auger electrons are taken into account as

well. However, the specific Auger structure of the emitted electron spectra is not reproduced by the treatment here.

B. General expression of the yield and the energy distribution

The discussion given here follows closely the one in Ref. 33. The initiating particle starts its motion in the plane $x=0$ at time $t=0$ with velocity $\vec{v}$ (Fig. 2). Let

$$G(x, \vec{v}_0, \vec{v}, t)\, d\vec{v}_0 dx \tag{1}$$

be the average number of electrons moving at time t in a layer $[x, x+dx]$ with velocity $[\vec{v}_0, \vec{v}_0 + d\vec{v}_0]$. Depending on the type of the impinging particle a subscript may be attached to G. e,t, or b correspond to an $e$lectron (mass m_e), an incident $t$arget atom (atomic number Z_2, atomic mass M_2) or an arbitrary $b$eam atom (atomic number Z_1, mass M_1), respectively. In order to simplify the notation, these three subscripts will be omitted in most cases.

The following evaluation is performed in three steps as sketched in Fig. 1. A determination of $G_{(b)}$ requires knowledge of $G_{(t)}$ and $G_{(e)}$, and a determination of $G_{(t)}$ requires again knowledge of $G_{(e)}$. The development in space and time of the electron cascade is taken into account by $G_{(e)}$; this must be determined first. Since the contribution to the cascade from recoiling target atoms may become appreciable, the second step must be an investigation of a medium where only target atoms and electrons participate in the cascade. Thus $G_{(t)}$ must be determined as the second step. Finally, $G_{(b)}$ can be determined. This step procedure is characteristic for the mathematical evaluation of transport equations governing radiation effects.[33,35,37]

We then obtain the number of emitted electrons J with velocities in the interval $[\vec{v}_0, \vec{v}_0 + d\vec{v}_0]$ in the backward direction through the plane at $x=0$, initiated by a single incident electron or atom with velocity $\vec{v}$. This is found by means of the function $G(x, \vec{v}_0, \vec{v}, t)$ from Eq. (1)

$$J(\vec{v}_0, \vec{v})\, d\vec{v}_0 = |v_{0x}| \left(\int_0^\infty dt\, G(0, \vec{v}_0, \vec{v}, t) \right) d\vec{v}_0 \ . \tag{2}$$

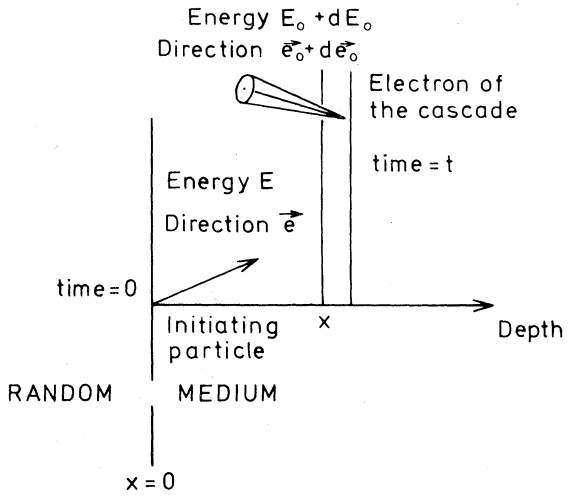

FIG. 2. Geometry for the quantity $G(x, \vec{v}_0, \vec{v}, t)\, d\vec{v}_0 dx$, Eq. (1).

$v_{0x} = v_0 \cos\theta_0$ is the x component of the velocity $\vec{v}_0$. From Eq. (2) the yield is determined by integration over all $\vec{v}_0$ which enable the electrons to eventually pass the surface barrier.

The essential point of Eq. (2) is that a determination of the velocity distribution or of the yield does not require knowledge of the specific time dependence of G. In view of this, it is sufficient to determine the slowing-down density

$$F(x, \vec{v}_0, \vec{v}) = \int_0^\infty G(x, \vec{v}_0, \vec{v}, t)\, dt \ . \tag{3}$$

A possible subscript is, of course, the same on both sides of the equation. $F(x, \vec{v}_0, \vec{v})\, |\vec{v}_{0x}|\, d\vec{v}_0$ is thus the total number of electrons that penetrate the plane x with a velocity $[\vec{v}_0, \vec{v}_0 + d\vec{v}_0]$ during the development of the cascade.

C. Equations for the functions G

Let N be the number density of target atoms in the medium, v_x the x component of the velocity $\vec{v}$, and $\vec{v}'$ and $\vec{v}''$ the velocities of the scattered and recoiling particles, respectively, after a collision.

$G_{(e)}$, $G_{(t)}$, and $G_{(b)}$ all satisfy a linear Boltzmann equation in backward form:

$$-\frac{v_x}{v}\frac{\partial G}{\partial x} - \frac{1}{v}\frac{\partial G}{\partial t} = N \int d\sigma \left[G(x, \vec{v}_0, \vec{v}, t) - G(x, \vec{v}_0, \vec{v}', t) - \sum_i G_{(e)i}(x, \vec{v}_0, \vec{v}_e'', t) - G_{(t)}(x, \vec{v}_0, \vec{v}_t'', t) \right] \ . \tag{4}$$

This equation may be derived by a standard argument.[33,35,37,45]

The cross section $d\sigma$ accounts for the collision probability of the primary particle with both a target nucleus and the associated Z_2 electrons,

$$d\sigma = d\sigma(\vec{v}, \vec{v}', \vec{v}_e'', \vec{v}_t'') \ . \tag{5}$$

It depends on the velocity of the primary particle before and after the collision, on the velocities $\vec{v}_e''$ of

the excited electrons, and on the velocity of the recoiling target atom $\vec{v}_t''$. In the following treatment the subscripts e, t, and i are dropped in the arguments of the functions G.

At $t=0$ and ∞, we must have

$$G_{(e)}(x,\vec{v}_0,\vec{v},0)=\delta(x)\delta(\vec{v}-\vec{v}_0)\ ,$$
$$G_{(t)}(x,\vec{v}_0,\vec{v},0)=0\ , \tag{6a}$$
$$G_{(b)}(x,\vec{v}_0,\vec{v},0)=0\ ,$$

and

$$G(x,\vec{v}_0,\vec{v},\infty)=0,\quad \text{for } \vec{v}_0\neq 0\ . \tag{6b}$$

In order to put Eq. (4) into a more convenient form, a procedure suggested by Lindhard *et al.*[35] will be utilized to separate collisions with target nuclei from those with electrons. The idea is that electronic excitation predominantly occurs at relatively large impact parameters where nuclear collisions are unimportant. This separation has turned out to be very useful for analyzing effects from incident ions. For incident electrons such a separation means merely that the electron is either scattered by the nucleus almost without any energy loss, or loses energy at some electronic excitation without being deflected by the nucleus. The cross section Eq. (5) is split into two components, $d\sigma_t$ for target nucleus collisions, and $d\sigma_e$ for electron collisions (Table I).

Hence, the integral in Eq. (4) can be separated into two collision integrals, and the following Boltzmann equation is obtained:

$$-\frac{v_x}{v}\frac{\partial G}{\partial x}-\frac{1}{v}\frac{\partial G}{\partial t}=N\int d\sigma_e\,[G(x,\vec{v}_0,\vec{v},t)-G(x,\vec{v}_0,\vec{v}',t)-G_{(e)}(x,\vec{v}_0,\vec{v}'',t)]$$
$$+N\int d\sigma_t\,[G(x,\vec{v}_0,\vec{v},t)-G(x,\vec{v}_0,\vec{v}',t)-G_{(t)}(x,\vec{v}_0,\vec{v}'',t)]\ . \tag{7}$$

D. Equations for the slowing-down density F

As mentioned above we are interested only in the slowing-down density F. Before considering all the equations for F we shall point out how the equation for $F_{(e)}$ simplifies.

TABLE I. The efficiency $\gamma=T_{\max}/E$ of energy transfer in a binary collision (the struck particle is initially at rest), power cross sections, and stopping powers.

Particle combination	Electron → electron	Electron → target nucleus	Beam ion → electron	Beam ion → target atom
Efficiency of energy transfer γ	1	$4\frac{m_e}{M_2}$	$4\frac{m_e}{M_1}$	$\frac{4M_1M_2}{(M_1+M_2)^2}$
Cross section	$d\sigma_e$	$d\sigma_t$	$d\sigma_e$	$d\sigma_t$
Model cross section	$CE^{-m'}T^{-1-m}dT$		$CE^{-m}T^{-1-m}dT$	$CE^{-m}T^{-1-m}dT$
Stopping power $NS(E)$	$\frac{NCE^{1-m-m'}}{(1-m)}$		$\frac{NC\gamma^{1-m}E^{1-2m}}{(1-m)}$	$\frac{NC\gamma^{1-m}E^{1-2m}}{(1-m)}$
Low-energy stopping power at energy E_0	$NS_{e,e}(E_0)$			

Let us for a moment exclusively regard $F_{(e)}(x, \vec{v}_0, \vec{v})$. The maximum energy transfer T_{max} from an incident electron of energy E to a target nucleus in rest is given in Table I. The energy transfer from a slow recoiling nucleus to an electron is even smaller, and the nucleus will be unable to liberate electrons. Hence, we can neglect the third team in the second integral in the equation for $F_{(e)}(x, \vec{v}_0, \vec{v})$,[35] so the equation for $F_{(e)}$ becomes decoupled.

By integrating Eq. (7) with respect to t three equations are obtained:

$$\frac{1}{v}\delta(x)\delta(\vec{v}-\vec{v}_0) - \frac{v_x}{v}\frac{\partial F_{(e)}}{\partial x} = N\int d\sigma_e [F_{(e)}(\vec{v}) - F_{(e)}(\vec{v}') - F_{(e)}(\vec{v}'')] + N\int d\sigma_t [F_{(e)}(\vec{v}) - F_{(e)}(\vec{v}')] \ , \tag{8a}$$

$$-\frac{v_x}{v}\frac{\partial F_{(t)}}{\partial x} = N\int d\sigma_e [F_{(t)}(\vec{v}) - F_{(t)}(\vec{v}') - F_{(e)}(\vec{v}'')] + N\int d\sigma_t [F_{(t)}(\vec{v}) - F_{(t)}(\vec{v}') - F_{(t)}(\vec{v}'')] \ , \tag{8b}$$

$$-\frac{v_x}{v}\frac{\partial F_{(b)}}{\partial x} = N\int d\sigma_e [F_{(b)}(\vec{v}) - F_{(b)}(\vec{v}') - F_{(e)}(\vec{v}'')] + N\int d\sigma_t [F_{(b)}(\vec{v}) - F_{(b)}(\vec{v}') - F_{(t)}(\vec{v}'')] \ . \tag{8c}$$

For convenience, the variables x and $\vec{v}_0$ have been omitted.

Even if $d\sigma$ were accurately known it would be quite difficult to solve the three integro-differential equations because of the large number of variables.

The solution $F_{(t)}$ is found by a two-step process, because $F_{(e)}$ must first be determined from Eq. (8a) and then be inserted in Eq. (8b). $F_{(b)}$ must be found by a similar three-step process.

III. EQUATIONS IN ENERGY VARIABLES

In order to solve Eq. (8) we shall follow a procedure described by Sigmund.[46] The velocity variables are changed to energy variables in a way such that

$$E_0 = \tfrac{1}{2}m_e v_0^2, \quad E = \tfrac{1}{2}M_A v^2 \ , \qquad \frac{\vec{v}_0}{|\vec{v}_0|} = \vec{e}_0, \quad \frac{\vec{v}}{|\vec{v}|} = \vec{e} \ , \tag{9}$$

where M_A is the mass of the primary particle, i.e., m_e, M_2, or M_1.

In order to remove the dependence on $\vec{e}$, $F(x, E_0, \vec{e}_0, E, \vec{e})$ is expanded in spherical harmonics

$$Y_{lk}(\vec{e}) = \left[\frac{2l+1}{4\pi}\right]^{1/2}\left[\frac{(l-|k|)!}{(l+|k|)!}\right]^{1/2} \times P_l^{|k|}(\cos\theta)e^{ik\alpha} \ . \tag{10}$$

We use the notation of Schiff,[47] where $P_l^{|k|}$ are generalized Legendre polynomials in the directional cosine of $\vec{e} = (\cos\theta, \sin\theta\cos\alpha, \sin\theta\sin\alpha)$. Then,

$$F(x, E_0, \vec{e}_0, E, \vec{e}) = \sum_{l=0}^{\infty}\sum_{k=-l}^{l} [4\pi(2l+1)]^{1/2} F_{lk}(x, E_0, \vec{e}_0, E)\, Y_{lk}(\vec{e}) \ , \tag{11}$$

where the coefficients $F_{lk}(x, E_0, \vec{e}_0, E)$ are determined by

$$F_{lk}(x, E_0, \vec{e}_0, E) = \frac{1}{[4\pi(2l+1)]^{1/2}}\int F(x, E_0, \vec{e}_0, E, \vec{e})\, Y_{lk}^*(\vec{e})\, d\vec{e} \ . \tag{12}$$

The conventional procedure in the theory of slowing down of ions involves the spatial moments of the density

$$F^n(E_0, \vec{e}_0, E, \vec{e}) = \int_{-\infty}^{\infty} x^n F(x, E_0, \vec{e}_0, E, \vec{e})\, dx \qquad (n = 0, 1, \ldots) \ . \tag{13}$$

The change to spatial moments leads, as shown below, to a recursion formula for the moments. Moreover, one notes that the introduction of the spatial moments eliminates the dependence on x.

We follow the procedure described in Refs. 37, 46, and 48. The directional dependence of the cross sections may be expressed in a simple way by energy quantities if the scattering angle ϕ' of the primary particle and the angle ϕ'' (with respect to the original direction of the primary particle) of the recoiling particle in the laboratory system are correlated to the primary energy, the energy E' after scattering, and

energy E'' of the recoiling particle. E' and E'' each refer to the laboratory system.

These correlations between angles and energies exist for elastic collisions at high primary velocities. We shall, therefore, assume that the velocity of the primary particle is so high that it strikes nuclei and electrons essentially *at rest.*

Hence, one obtains a set of equations for the spherical coefficients $F_{lk}^{n}(E)$, from which the variables E_0 and $\vec{e}_0$ have been removed for convenience for all three cases of incidence:

$$N(2l+1)\int d\sigma_e\,[F_{lk}^{n}(E)-P_l(\cos\phi')F_{lk}^{n}(E')-P_l(\cos\phi'')F_{(e)lk}^{n}(E'')]$$
$$+N(2l+1)\int d\sigma_t\,[F_{lk}^{n}(E)-P_l(\cos\phi')F_{lk}^{n}(E')-P_l(\cos\phi'')F_{(t)lk}^{n}(E'')]$$
$$=n(l^2-k^2)^{1/2}F_{l-1,k}^{n-1}(E)+n[(l+1)^2-k^2]^{1/2}F_{l+1,k}^{n-1}(E)+\delta_{n0}\frac{1}{v}\delta(E-E_0)\left[\frac{2l+1}{4\pi}\right]^{1/2}Y_{lk}^{*}(\vec{e}_0)$$
$$(n=0,1,\ldots)\ . \qquad (14)$$

As mentioned in Sec. II the third term in the second integral disappears in the equations for the moments of $F_{(e)}$, and the term containing the Kronecker symbol δ_{n0} will be present only for the zeroth-order moment of $F_{(e)}$.

In Eq. (14) the spatial moments are determined recurrently from the lower moments on the right-hand side of the equation. Let us finally express the angles ϕ' and ϕ'' in the laboratory system in terms of the primary energy E and the energy transfer T.

For the scattering angle ϕ' in the laboratory system of a collision between the primary particle (mass M_A) and a target particle (mass M_B) at rest we apply the expression from binary elastic collisions in classical mechanics[49]

$$\cos\phi'=\left[1-\frac{T}{E}\right]^{1/2}+\tfrac{1}{2}\left[1-\frac{M_B}{M_A}\right]\left[\frac{T}{E}\right]\left[1-\frac{T}{E}\right]^{-1/2}\ , \qquad (15)$$

and for the angle ϕ'' of the recoiling particle

$$\cos\phi''=\left[\frac{T}{T_{\max}}\right]^{1/2}=\left[\frac{T}{\gamma E}\right]^{1/2}\ , \qquad (16)$$

where γ is indicated in Table I.

IV. COLLISION CROSS SECTIONS AND STOPPING POWERS

In order to treat the possible collisions we shall make extensive use of model cross sections (general power cross sections). These are introduced for analytical convenience; whenever possible the final results are expressed by quantities available from experiments or from theoretical evaluations other than this one. Usually it is not possible to eliminate the complete dependence on the exponents from the final results. However, it turns out that this dependence usually is comparatively weak.

A. Energy-transfer cross sections and the related stopping powers

Before considering the general case let us regard a collision between an incident beam ion and a target atom at rest. From the power-law potential[50]

$$V(R)\sim R^{-1/m}\ , \qquad (17)$$

where R is the distance of separation, a simple power cross section

$$d\sigma_t=CE^{-m}T^{-1-m}dT \qquad (18)$$

has been derived.[50] T is the kinetic energy of the recoiling target atom, and C a constant which depends on the charges and masses of the particles as well as on the exponent m.

We shall in the following treatment often use the corresponding (nuclear) stopping power:

$$-\left[\frac{dE}{dx}\right]_t=NS_t(E)=N\int_0^{T_{\max}}d\sigma_t\,T\ . \qquad (19)$$

The *atomic* stopping cross section then becomes

$$S_t(E)=C\frac{\gamma^{1-m}}{1-m}E^{1-2m}\ . \qquad (20)$$

Similar power cross sections will now be utilized for all collisions between the considered particles. These cross sections and their corresponding stopping powers are listed in Table I. In order to distinguish between the exponents from the different cross sections it may become necessary to use subscripts on the exponents. The cross section for an electron-electron interaction is an extension of Eq. (18), as m' may differ from m.

B. Connection between screening and power cross sections

Over appreciable regions of the separation distance the screened potential may usually be approximated

by a power law steeper than R^{-1}. The cross section Eq. (18) will become more and more forward peaked with increasing values of the exponent m in the approximation for the screened potential Eq. (17).[51] m increases with rising energy up to $m=1$ at which the cross section becomes identical with a Rutherford cross section.

C. Feasibility of the model cross sections

The power cross section for *beam-ion–target-atom* collisions and for *beam-ion–electron* collisions and the corresponding stopping powers $NS_t(E)$ and $NS_e(E)$ are available from existing theories over wide ranges of energy or known from experimental data. Therefore, the power cross sections for $d\sigma_t$ and for $d\sigma_e$ will be used only for analytical convenience. The power cross section for $d\sigma_t$ with fixed values of m equal to 0.05, $\frac{1}{4}$, $\frac{1}{3}$, or $\frac{1}{2}$ has already been utilized widely in the literature[33,35,37]; the appropriate interval for the m values becomes here [0,1]. Correspondingly, the electronic stopping power for an incident ion varies with decreasing energy from a stopping power inversely proportional to the squared velocity to one proportional to the velocity. This leads to values of the exponent m in the interval $[\frac{1}{4},1]$.

Power cross sections similar to Eq. (18) for the *electron-electron* collisions and the *electron-nucleus* collisions have been used by Kanaya and Okayama,[52] who evaluated the electron range and other related penetration quantities. In order to obtain satisfactory agreement with experimental results they used fixed exponents $m=m'=\frac{5}{6}$. In a subsequent article[30] the electron range and a relative secondary electron yield were calculated for some discrete values of m in the interval $[\frac{1}{2},\frac{5}{6}]$. The present model cross section $d\sigma_e$ in Table I is slightly more flexible in that the exponents m and m' are both free parameters. However, since the value of m' turns out to be uncritical, the choice $m'=m$ is used in all comparisons with existing stopping powers for electrons. In the evaluation of the slowing-down density $F_{(e)}$ the more general expression in Table I is applied.

Values of m in the interval $[-1,1]$ cover the range of stopping powers from one proportional to E^3 down to E^{-1}. The existing calculations of the stopping power show actually such a range of energy dependence, although the stopping powers below their maximum of around 100 eV are rather uncertain.[53] It turns out that extracted values of m (with $m=m'$) from the theoretical calculations or from experimental secondary electron energy spectra, discussed in Sec. IX, even lie below -1 at very low energies, i.e., a few eV above the vacuum level.

A generalized power cross section, which to some extent includes exchange corrections, is introduced in Ref. 45, and the corresponding stopping power is evaluated.

D. Theoretical stopping powers for beam atoms

The results for the nuclear and electronic stopping power for an incident beam atom from the work of Lindhard *et al.*[35,50,54] will briefly be mentioned.

The nuclear stopping power for all beam-target combinations can reasonably be described[50] by a universal dimensionless function, $s_n(\epsilon)$, defined by the equation

$$s_n(\epsilon)=NS_t(E)\frac{M_1+M_2}{N4\pi e^2 a Z_1 Z_2 M_1} , \tag{21}$$

where the reduced dimensionless energy parameter ϵ is determined by the relation:

$$\epsilon=E\frac{aM_2}{Z_1Z_2e^2(M_1+M_2)} . \tag{22}$$

The screening radius a is expressed by means of the Bohr radius a_0 as

$$a=0.8853a_0(Z_1^{2/3}+Z_2^{2/3})^{-1/2} . \tag{23}$$

If one requires $\sim 20\%$ accuracy in the nuclear stopping the power cross section Eq. (18) may be used[37] with

$$m=\begin{cases}\frac{1}{3} & \text{for } \epsilon \lesssim 0.2,\\ \frac{1}{2} & \text{for } 0.08 \lesssim \epsilon \lesssim 2.0 .\end{cases} \tag{24}$$

According to Lindhard *et al.*[35,54] the electronic stopping power for an ion can be approximated by the dimensionless function

$$s_e(\epsilon)=k_L\epsilon^{1/2} , \tag{25}$$

for $E \lesssim Z_1^{4/3}A_1 25$ keV; here A_1 is the mass number of the beam ion, and k_L is a well-defined constant depending on Z_1 and Z_2, and of the order of 0.1 to 0.2 except for $Z_1 \ll Z_2$, where k_L can become larger than 1. This stopping corresponds to the velocity-proportional electronic stopping power, which may be written with an associated constant k:

$$NS_e(E)=NkE^{1/2} . \tag{26}$$

V. EVALUATION OF THE ZEROTH-ORDER MOMENT OF THE DENSITY $F_{(e)}$

In this section let us exclusively treat the density $F_{(e)}$, initiated by an incident electron. The subscript e and the variables E_0 and $\vec{e}_0$ will be mostly neglected here.

The equations that determine the coefficients for the zeroth-order moment F^0 are investigated here. For the mathematical solution of Eq. (14) it is important that energy conservation leads to the following threshold condition:

$$F(x,E_0,\vec{e}_0,E,\vec{e})=0 \quad \text{for } E<E_0 \ , \tag{27}$$

and this must also be valid for all coefficients in the spherical expansion

$$F_{lk}^n(E_0,\vec{e}_0,E)=0 \quad \text{for } E<E_0 \ . \tag{28}$$

It has been demonstrated in similar integral equations[46,55] with a binding energy V that the leading term for $E >> E_0 >> V$ in the solution is identical to the leading term for $E >> E_0$ in the solution of the corresponding equation with $V=0$. We then set

$$E'=E-T \quad \text{and} \quad E''=T \ , \tag{29}$$

and obtain from Eq. (14) with $n=0$ the equations which determine the coefficients of the zeroth-order moment:

$$N(2l+1)\int d\sigma_e[F_{lk}^0(E)-P_l(\cos\phi')F_{lk}^0(E-T)-P_l(\cos\phi'')F_{lk}^0(T)]$$
$$+N(2l+1)\int d\sigma_t[F_{lk}^0(E)-P_l(\cos\phi')F_{lk}^0(E-T)]=\frac{1}{v}\delta(E-E_0)\left[\frac{2l+1}{4\pi}\right]^{1/2}Y_{lk}^*(\vec{e}_0) \ . \tag{30}$$

The integral equations (30) are more complex than those describing sputtering and problems concerning recoiling atoms,[33,39] and which could all be rearranged in such a way that they contained only one explicit collision integral. This is usually not the case in the present equations.

Setting $l=0$ and utilizing $P_0(\cos\phi)=1$, we may evaluate the coefficient $F_{00}^0(E)$ from Eq. (30):

$$N\int d\sigma_e[F_{00}^0(E)-F_{00}^0(E-T)-F_{00}^0(T)]$$
$$+N\int d\sigma_t[F_{00}^0(E)-F_{00}^0(E-T)]$$
$$=\frac{1}{v}\delta(E-E_0)\frac{1}{(4\pi)^{1/2}}Y_{00}^*(\vec{e}_0) \ . \tag{31}$$

Because of the low energy transfer from the impinging electron to the scattering nucleus we may use a first-order expansion in T in the second integral as described elsewhere[56,57]:

$$N\int d\sigma_e[F_{00}^0(E)-F_{00}^0(E-T)-F_{00}^0(T)]$$
$$+NS_t(E)\frac{d}{dE}F_{00}^0(E)$$
$$=\frac{\delta(E-E_0)}{v}\frac{Y_{00}^*(\vec{e}_0)}{(4\pi)^{1/2}} \ . \tag{32}$$

In order to evaluate F_{00}^0 we even may neglect the second term on the left-hand side, because the nuclear stopping power $NS_t(E)$ is orders of magnitude smaller than the electronic stopping power $NS_e(E)$ which implicitly enters into the first integral.[16]

Let us now insert the power cross section for $d\sigma_e$ (Table I) in Eq. (32) and introduce a logarithmic variable $u=\ln E/E_0$. We make use of the technique described in Refs. 58 and 55 and utilize condition (28) to obtain the exact Laplace transform of $F_{00}^0(E_0e^u)$ with respect to u:

$$\tilde{F}_{00}^0(s)=\int_0^\infty du\, e^{-su}F_{00}^0(E_0e^u)$$
$$=-m(s-m)/\left[s-\frac{\Gamma(s+1)\Gamma(1-m)}{\Gamma(s-m)}\right]$$
$$\times\frac{E_0^{m+m'-1}}{v_0NC}\frac{Y_{00}^*(\vec{e}_0)}{(4\pi)^{1/2}} \ . \tag{33}$$

An exact inversion from the Laplace space of $\tilde{F}_{00}^0(s)$ is not known. An asymptotic expansion for $E >> E_0$ of the form[59]

$$F_{00}^0(E)\approx\sum_{s_j}A_{s_j}e^{s_ju}=\sum_{s_j}A_{s_j}\left[\frac{E}{E_0}\right]^{s_j} \tag{34}$$

can be found with real exponents s_j in descending order; Laplace transform of Eq. (34) yields

$$\tilde{F}_{00}^0(s)=\sum_{s_j}\frac{A_{s_j}}{s-s_j} \ . \tag{35}$$

This means that the exponents s_j of the expansion Eq. (34) are the poles of $\tilde{F}_{00}^0(s)$ and the coefficients A_{s_j} are the residues. The highest pole is $s_1=1$, and from the behavior of the Γ function the next highest pole is seen to be negative. Neglecting all terms originating from negative poles, we can invert $\tilde{F}_{00}^{00}(s)$ to

$$F_{00}^0(E)\approx\Gamma_m\frac{E_0^{m+m'-1}}{v_0NC}\left[\frac{E}{E_0}\right]\frac{Y_{00}^*(\vec{e}_0)}{(4\pi)^{1/2}} \tag{36}$$

for $E >> E_0$,

where

$$\psi(x)=\frac{d}{dx}\ln\Gamma(x) \ , \tag{37}$$

and

$$\Gamma_m = \frac{m}{\psi(1) - \psi(1-m)} \quad . \tag{38}$$

Using the stopping power (Table I), we rewrite Eq. (36)

$$F^0_{(e)00}(E) \approx \Gamma_m \frac{(E/E_0)}{v_0 N S_{e,e}(E_0)} \frac{Y^*_{00}(\vec{e}_0)}{(4\pi)^{1/2}} \tag{39}$$

for $E >> E_0$.

Here we inserted the stopping power $NS_{e,e}(E_0)$ of the liberated electron at the instantaneous energy E_0 to remove most of the explicit m dependence. Apart from Γ_m, which is a slowly varying function of m for $m \leq 1$, Eq. (39) contains no quantities indicative of a power cross section.

It is central to the calculation that m and C are determined from the low-energy stopping power $NS_{e,e}(E_0)$ because of the arguments from sputtering.[33]

The terms $F^0_{(e)lk}$ for $l \geq 1$ will be neglected in the zeroth-order moment of $F_{(e)}$. Generally the scattering nuclei will cause this *isotropic approximation* to be much better than the corresponding approximation in sputtering. This may be explained as follows: For all the coefficients $F^0_{(e)lk}$ we may arrive at expressions analogous to those obtained for self-sputtering,[33,46] if we consider electron impact on a pure electron medium, i.e., a medium without scattering nuclei. The coefficients F^0_{lk} for $l \geq 1$ have already been neglected in sputtering.[33] Consequently the terms $F^0_{(e)lk}(l \geq 1)$ for a real medium can be disregarded with even much less error relative to the isotropic approximation.

In Ref. 45 the coefficients $F^0_{(e)1k}$ have been determined for a specific example of $d\sigma_t$ by a procedure similar to that used on Eq. (31). It appears that they indeed are small compared with $F^0_{(e)00}(E)$.

We obtain, then, for the zeroth-order moment in the isotropic approximation

$$F^0_{(e)}(E_0, \vec{e}_0, E, \vec{e}) \approx \frac{\Gamma_m}{4\pi} \frac{(E/E_0)}{v_0 N S_{e,e}(E_0)} = \chi E \quad . \tag{40}$$

In this approximation for the zeroth-order moment we note that χ depends only on the properties of the liberated electrons, and *not* on any quantities pertaining to the primary electron.

VI. CONNECTION BETWEEN $F_{(e)}$ AND THE SPATIAL ENERGY DISTRIBUTION $D_{(e)}$

A. Spatial energy distribution $D_{(e)}(x, E, \vec{e})$

The spatial distribution of energy, given to the target electrons has been determined experimentally, theoretically, or by means of Monte Carlo calculations by a number of authors.

Comprehensive measurements of the distribution in air by means of luminescence radiation were performed in pioneering work by Grün[60] for primary electron energies from 5 to 54 keV. This experimental distribution is essentially determined from the location of ionized nitrogen molecules. In later experiments with nitrogen[61,62] Grün's procedure has been extended down to primary energies of 300 eV.

Everhart and Hoff[63] measured the depth distribution of the charge-carrier pair generation in a system of aluminum, silicon dioxide, and silicon bombarded by 6–20-keV electrons. Their results agreed well with Grün's data and with the calculated distribution by Spencer[64] described below.

Theoretical evaluations were performed by Spencer,[64,65] who calculated the energy-loss distribution for primary energies larger than 25 keV in various materials. Evaluations have recently been made[66] for low primary energies in water. In this distribution the contribution from recoiling ionized electrons has been entirely neglected, but since the energy distribution of the ionized electrons is strongly peaked at low energies for primary energies in the Rutherford region, this energy-loss distribution is expected to provide useful estimates for the energy distribution in the energy range considered by Spencer and somewhat below these energies. At 32 keV his distribution appeared to agree well with that of Grün found experimentally.

Several Monte Carlo calculations have been performed in various media. Berger *et al.*[67] followed keV electrons, including the secondaries, down to 200 eV in air and computed the distribution on the basis of Bethe's stopping-power expression. Their distribution agreed well with the results of Grün and Spencer's calculations for 32-keV electrons in air. On the other hand, Grosswendt and Waibel[68] computed the distribution in air on the basis of knowledge of the location of the excitations and ionizations and obtained reasonable agreement with experimental results. Shimizu *et al.*[69] and Matsukawa *et al.*[70] performed calculations for energy-loss distributions for 10- and 30-keV electrons incident on several metals and carbon, and obtained agreement with the distribution of Everhart and Hoff[63] as well as Spencer.[64] Paretzke[71] obtained good agreement with the distribution found by Grün for 5- and 10-keV electrons on water.

Four examples of the energy distribution in air are shown in Fig. 3. This figure illustrates a well-documented feature[60,63,71] that the distribution, in units of the stopping power $NS_e(E)$ and the range of the primary electron, is relatively insensitive to changes in the primary energy. The energy distribution is approximated rather well by a step function with a discontinuity of magnitude $NS_e(E)$ in the

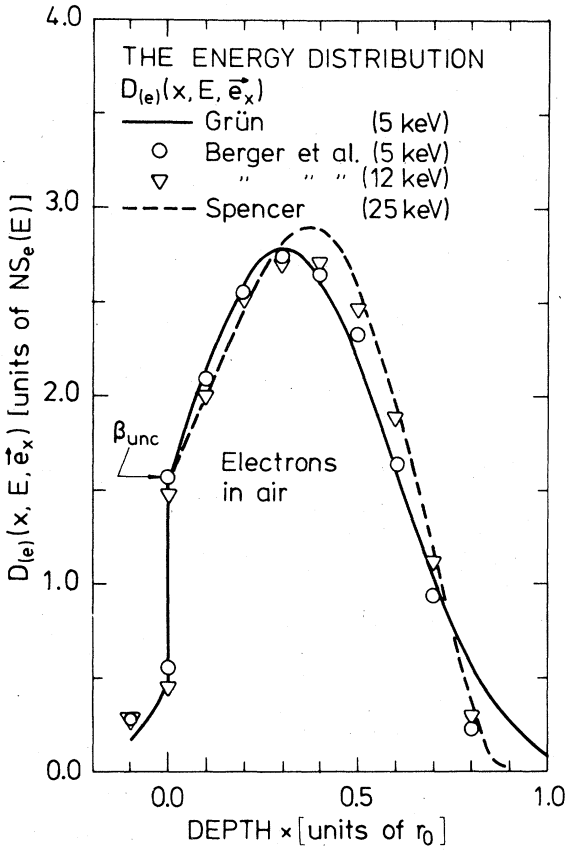

FIG. 3. Energy distribution $D_{(e)}(x,E,\vec{e}_x)$ for an infinite air medium resulting from keV electrons which initiate their motion at $x=0$ and with a direction $\vec{e}_x$ along the x axis. The distribution is plotted in units of the stopping power $NS_e(E)$ for the primary electron as a function of the depth in units of the mean range r_0, Ref. 67. (——), experimental curve, Ref. 60; (– – –), theoretical curve, Ref. 64; (0) and (▽), Monte Carlo calculations (model B), Ref. 67. β_{unc} indicates the upper value of the distribution at the step $x=0$.

plane, $x=0$, where the primaries initiate their motion.[63–65] The origin of this discontinuity is the following: primary particles in the beginning of their motion deposit energy only in the region $x \geq 0$ of the infinite medium. This discontinuity was clearly observed by Grün[60] and by Cohn and Caledonia,[61] although the real experimental values around the plane $x=0$ show a steep increase for increasing x rather than a discontinuity at the surface.

Figure 3 demonstrates as well that the upper value of the step function at $x=0$ given in units of $NS_e(E)$ is almost constant. The value is indicated in the figure by β_{unc} (where the subscript means uncorrected for energy transport by recoiling electrons at the surface, cf. Sec. X C). Grün[60] found experimentally that β_{unc} varied less than 10% in air for primary electron energies in the 5- to 54-keV range. Also Barrett and Hays[62] found a small variation of β_{unc} in their data for nitrogen of 1 to 3 keV. Spencer's calculations[64,65] support these results for a number of materials and primary energies from 25 keV and upwards. Apart from the results of Barrett and Hays β_{unc} in these examples refers to a medium in which the distribution also has been determined for negative depths behind the electron source at $x=0$.

A corresponding slow variation of β_{unc} for a semi-infinite air medium has been demonstrated by Berger *et al.*[67] β_{unc} decreased by 10% with increasing primary electron energy from 2 to 20 keV.

B. Basic equations for the energy distribution

The energy distribution $D_{(e)}(x,E,\vec{e})$ from an incident electron with energy E and direction $\vec{e}$ satisfies a Boltzmann equation similar to the one given in Ref. 42. The distribution $D_{(e)}$ is normalized by

$$D^0(E,\vec{e}) = \int_{-\infty}^{\infty} D(x,E,\vec{e})\,dx = E \quad , \tag{41}$$

since the energy from a primary electron nearly exclusively ends up in electronic excitation according to the discussion in Sec. II. Following the same procedure as used in Sec. II and III, we obtain an equation for the coefficients $D^n_{(e)l}(E)$:

$$N(2l+1)\int d\sigma_e\,[D_l^n(E) - P_l(\cos\phi')D_l^n(E') - P_l(\cos\phi'')D_l^n(E'')]$$

$$+N(2l+1)\int d\sigma_t\,[D_l^n(E) - P_l(\cos\phi')D_l^n(E')]$$

$$= n(l^2-k^2)^{1/2}D_{l-1}^{n-1}(E) + n[(l+1)^2-k^2]^{1/2}D_{l+1}^{n-1}(E) \qquad (n=1,2\cdots) \quad . \tag{42}$$

In this section we shall mainly neglect the subscript e. The coefficients for the energy distribution D are obviously simpler than those for F, as D contains only one directional variable $\vec{e}$. As a consequence, the directional expansion is characterized by a single subscript l.

An analogous equation for energy deposition by atomic particles is well known and extensively discussed in

Ref. 37. The arguments leading to Eq. (42) are entirely analogous to those for atomic particles.

C. Factorization of the slowing-down density

According to the final result in Sec. V, the zeroth-order moment of the slowing-down density F is proportional to the primary energy E by the quantity

$$\chi = \frac{\Gamma_m(1/E_0)}{v_0 N S_{e,e}(E_0) 4\pi} \quad . \tag{43}$$

As the zeroth-order moment of the energy distribution D is the primary energy E, Eq. (41), a comparison between D and F/χ presents itself. Let us for a moment ignore the threshold conditions (27) and (28) and consider the coefficients of the directional expansion.

The coefficients to the zeroth-order moment of the distribution D are determined[37] by

$$D_l^0(E) = E\delta_{0l} \quad , \tag{44}$$

whereas the corresponding coefficients for F/χ in the isotropic approximation read

$$F_{lk}^0(E)/\chi = E\delta_{0l}\delta_{0k} \quad . \tag{45}$$

Once all the coefficients F_{lk}^0 with $l \geq 1$ have been set equal to zero, Eq. (14) infers that only the coefficients F_{lk}^n of the higher-order moments with $k = 0$ will differ from zero. Then the subscript k can be omitted from the coefficients $F_{lk}^n(E)/\chi$.

Inserting $F_l^n(E)/\chi$ for $n \geq 1$ in Eq. (14), one obtains a system of equations which is completely identical to the system Eq. (42) that determines the coefficients $D_l^n(E)$. Since the coefficients for all moments of F/χ and D are equal, F can thus be factored as

$$F(x, E_0, \vec{e}_0, E, \vec{e}) = \chi D(x, E, \vec{e}) \tag{46}$$

for $E \gg E_0$. In fact, this factorization is analogous to the one performed in sputtering.[33]

D. Application of energy distribution to slowing-down density

The energy distribution D in Eqs. (42) and (46) is a spatial distribution of kinetic energy of the low-energy electrons. According to Ref. 37 the spatial distribution of ionization will be proportional to this distribution. Obviously, the experimental distribution and the distribution from Grosswendt and Waibel[68] then represent an energy distribution of this kind. Also, the energy-loss distribution can be utilized as a reasonable approximation to the distribution of kinetic energy so long as the primary energy is well above the eV region.

It seems straightforward, therefore, to apply this energy distribution to the slowing-down density F by means of the factorization in Eq. (46). This connection has not been utilized previously in secondary electron emission studies.

VII. ENERGY DEPOSITION BY ATOMIC PARTICLES

In this section we shall treat only the spatial distribution of energy deposition by atomic particles. Only the equations for the beam quantities, subscript b, will be given. The equations for the corresponding target quantities are obtained by replacement of the subscripts b by t.

Lindhard *et al.*[35] showed that the amount of energy which ultimately is lost to the electrons $\eta_{(b)}(E)$, and the energy delivered to the nuclei $\nu_{(b)}(E)$, are both described by integral equations. The energy $\nu_{(b)}$ obeys the equation

$$\int d\sigma_t [\nu_{(b)}(E) - \nu_{(b)}(E-T) - \nu_{(t)}(T)] + S_e(E)\frac{d\nu_{(b)}}{dE} = 0 \quad , \tag{47}$$

and is determined from the initial condition

$$\frac{\nu_{(b)}(E)}{E} \to 1 \quad \text{for } E \to 0 \quad . \tag{48}$$

Some approximations similar to those in Sec. V have already entered Eq. (47). The energy $\eta_{(b)}(E)$ is found from

$$\eta_{(b)}(E) = E - \nu_{(b)}(E) \quad . \tag{49}$$

The two quantities $\nu_{(b)}$ and $\eta_{(b)}$ are the zeroth-order moments of the spatial energy distributions. In particular

$$\eta_{(b)} = D_{(b)}^0 \quad . \tag{50}$$

The distributions of energy deposited in atomic motion or ionization have been extensively computed by Brice[38] and Winterbon,[39] respectively, for high and low beam energies. The former distribution will usually be called damage distribution here. As described in Sec. VIII, the knowledge of these distributions will be utilized whenever possible.

VIII. DISTRIBUTIONS $F_{(t)}$ AND $F_{(b)}$

This section deals with the distributions $F_{(t)}$ and $F_{(b)}$ initiated by a target atom or beam atom, respectively. In this section the intention is to show that a factorization corresponding to Eq. (46) is also possible for these distributions, and then investigate the role of the recoiling electrons for these distributions. We keep the notation of the preceding section and

write only the equations determining the beam quantities.

A. Solution for the zeroth-order moment $F^0_{(b)}(E)$

From Eq. (14) we obtain the equation determining the coefficient $F^0_{(b)00}$. In both integrals we neglect any binding energy for the recoils. As in the treatment of $F^0_{(e)00}$ in Sec. V we again perform a first-order expansion in T in the first integral, which concerns the atom-electron collisions. This is justified because of the low-energy transfer T from the atom to the recoiling electron. We therefore obtain for the first two terms in the integral:

$$\int d\sigma_e [F^0_{(b)00}(E) - F^0_{(b)00}(E-T)] \approx \int d\sigma_e \, T \frac{dF^0_{(b)00}}{dE} = \frac{dF^0_{(b)00}}{dE} S_e(E) \quad . \tag{51}$$

Using the result from Sec. V [Eqs. (39) and (40)], we obtain an equation for $F^0_{(b)00}$:

$$N \int d\sigma_t [F^0_{(b)00}(E) - F^0_{(b)00}(E-T) - F^0_{(t)00}(T)] = NS_e(E) \left[\chi - \frac{dF^0_{(b)00}}{dE} \right] \quad , \tag{52}$$

with the threshold condition for all n, l, k, similar to Eq. (28)

$$F^n_{(b)lk}(E_0, \vec{e}_0, E) = 0 \quad \text{for } \gamma E < E_0 \quad . \tag{53}$$

Combining Eqs. (47) and (49) one finds that Eq. (52) is identical to the equation which determines the energy $\eta_{(b)}(E)$ ultimately lost to the electrons, if

$$F^0_{(b)00} = \chi \eta_{(b)} \quad . \tag{54}$$

The results of Sec. V indicated that we could neglect all terms with $l \geq 1$ in $F^0_{(e)}$. This means that the equations for $F^0_{(b)lk}$ ($l \geq 1$) are satisfied by a zero solution $F^0_{(b)lk} = 0$. We obtain therefore

$$F^0_{(b)}(E) = \chi \eta_{(b)}(E) \quad . \tag{55}$$

Equation (55) means that the velocity distribution of the recoiling electrons is isotropic. This distribution is the result of many generations of recoiling electrons for $E >> E_0$.

B. Connection between $F_{(b)}(E)$ and $D_{(b)}(E)$

Let us now continue to generalize the factorization Eq. (55) from the zeroth-order moments to the proper distribution. One notices from Eqs. (54) and (55) that only coefficients $F^n_{(b)lk}$ with $k = 0$ will, according to Eq. (14), be different from zero. Hence the subscript k becomes redundant and will, therefore, be neglected at this point.

If the ansatz

$$F^n_{(b)l}(E) = \chi D^n_{(b)l}(E) \tag{56}$$

is inserted for all n and l in Eq. (14), the coefficients $D^n_{(b)l}(E)$ will be governed by the same system of equations. These equations are identical to those equations that may be derived directly for the spatial moments of the distribution $D_{(b)}$ of energy that is ultimately delivered to the target electrons. The system of equations is, of course, analogous to the system Eq. (42). The basic equation for this energy distribution is explicitly given in Ref. 42, and the arguments leading to this equation are the same as those for the previously mentioned cases.[37,39] The rest is completely analogous to the discussion of the distribution initiated by a primary electron in Sec. VI. We conclude, therefore, that

$$F_{(b)}(x, E_0, \vec{e}_0, E, \vec{e}) = \chi D_{(b)}(x, E, \vec{e}) \tag{57}$$

for $E >> E_0$.

C. Influence of the recoiling electrons on the energy distribution

The use of the tabulations of Brice[38] and Winterbon[39] is feasible only if their omission of the contribution from the recoiling electrons influences the energy distribution weakly. First, the significance of the recoiling electrons for the energy distribution $D_{(b)}$ is discussed qualitatively; following this, an example is presented.

Obviously, the recoiling electrons of low energy are able to migrate over only small depths compared with the range of the primary beam atom because of scattering on both electrons and nuclei. These electrons will, therefore, not change the energy deposition profile.

In an elastic (classical) beam atom-electron collision the most energetic recoil electron after the collision will reach approximately twice the velocity of the incident atom. As the stopping power for an electron is comparable in magnitude with that of an atom of the same velocity, the range of the ion will exceed the range along the path of the recoil electron with orders of magnitude. Furthermore, the scattering probability for an electron is much larger than the corresponding scattering probability for an atom with the same velocity, and that will diminish even more the possible migration depth for the recoiling electrons. The recoil spectrum is usually peaked at the low energies, and the energy deposited directly into low-energy electron excitations is thus larger than or

comparable to the energy deposited by fast recoil electrons.

These considerations, which do not include electron promotion, mean that the contribution from these fast recoiling electrons only will appear as corrections over a small length scale (of the order of the electron range) compared with the total range of the ion. On the other hand, the range of the most energetic recoil electrons may become more than one order of magnitude larger than the escape depth for the secondary electrons. However, it thus seems reasonable to neglect the recoil electrons in $D_{(b)}$ so long as we consider overall features of the profile and not the detailed behavior of $D_{(b)}$ near the surface. This is analogous to the similar considerations on the distribution of energy deposited in atomic motion.[72]

In the zeroth-order moment of energy distribution it is, however, not possible to neglect the contribution from the recoiling electrons. If it were, the term corresponding to $NS_e(E)\chi$ in Eq. (52) would be missing in the equation for $D^0_{(b)0}(E)$. In this case the factorization Eq. (55) would be invalid.

D. Estimate of the quantitative influence of the recoil electrons

Let us now more quantitatively consider the contributions from recoiling electrons. We can infer from Eq. (14) that if the recoiling electrons may be neglected for $n=1$ in the equations for $F^1_{(b)l}$, we would expect the contributions from these electrons to also play a minor role in higher moments ($n>1$). For $(n,l)=(1,1)$ we obtain from Eq. (14) the equation that determines $F^1_{(b)1}(E)$:

$$3N\int d\sigma_e\,[F^1_{(b)1}(E)-\cos\phi' F^1_{(b)1}(E-T)]+3N\int d\sigma_t\,[F^1_{(b)1}(E)-\cos\phi' F^1_{(b)1}(E-T)-\cos\phi'' F^1_{(t)1}(T)]$$
$$=\chi\eta_{(b)}(E)+3N\int d\sigma_e\cos\phi'' F^1_{(e)1}(T)\ . \quad (58)$$

The contribution of the recoiling electrons are represented by the integral on the right-hand side.

Let us consider the simple case (Ref. 45) of an energy-independent ratio between the electronic stopping power and the nuclear stopping power for an electron. The solution to Eq. (14) for $F^1_{(e)1}(E)$ is then

$$F^1_{(e)1}(E)=\chi A^1_{(e)1}\frac{E^{2m}}{NC} \quad (59)$$

[where the threshold condition (27) has been neglected]. C and m originate from the power cross section (Table I) of an electron-electron collision. $A^1_{(e)1}$ is a constant, which is evaluated by the procedure described in Ref. 37. An upper limit for $A^1_{(e)1}$ corresponding to a medium without nuclei is found in this reference. For practical reasons the quantity $A^1_{(e)1}/(1-m)$ is evaluated. This quantity varies from around 0.2 to 0.1 for m varying in the interval $[\frac{1}{2},1]$. As the exponent m in Eq. (59) must account for the range of the electron, this interval is realistic for electron energies above 100 eV.

The integral for the recoil contribution is now evaluated by means of the power cross section for a collision between a beam atom and a target electron with a constant C_b and an exponent m_b.

$$3N\int d\sigma_e\cos\phi'' F^1_{(e)1}(T)=3\chi NA^1_{(e)1}\int_0^{\gamma E}\frac{C_b\,dT}{E^{m_b}T^{1+m_b}}\left(\frac{T}{T_{\max}}\right)^{1/2}\frac{T^{2m+1}}{NC}$$
$$=3\chi\frac{A^1_{(e)1}}{(1-m)}\frac{(1-m_b)NS_e(E)}{(\frac{3}{2}+2m-m_b)NS_e(\gamma E)}\gamma E\ . \quad (60)$$

In Eq. (60) the electronic stopping power $NS_e(E)$ for an incident beam atom and the electronic stopping power $NS_e(\gamma E)$ of the most energetic recoil electron have been inserted. As was noted in Sec. VIII C these stopping powers are comparable in magnitude. The fraction $(1-m_b)/(\frac{3}{2}+2m-m_b)$ will, for feasible values of m_b corresponding to the interval $[\frac{1}{4},1]$, vary from $\frac{1}{3}$ to 0 and the upper limit for $A^1_{(e)1}/(1-m)$ will vary as described above. We, therefore, conclude that the integral will be at least two orders of magnitude less than the product $\gamma 3\chi E$, which is already very small relative to χE because of the low value of γ.

The competing term η on the right-hand side of Eq. (58) will behave as

$$\chi\eta_{(b)}(E)\approx\chi E\ . \quad (61)$$

This is asymptotic for large E since Lindhard *et al.*[35] showed that the asymptotic limit for $\eta_{(b)}(E)$ is E. By interpolating Winterbon's tabulations[39] we find for

$\epsilon \geq 100$: $\eta_{(b)}(E) \gtrsim 0.8E$ (ranging in mass ratio M_2/M_1 from $\frac{1}{25}$ to 25 for even the lowest realistic electronic stopping powers). In view of this we can conclude that the contribution from the recoiling electrons on the first spatial moment is negligible compared with the term (61) for energies at which the assumption of a correlation between energy transfer and scattering angle is valid.

IX. ENERGY AND ANGULAR DISTRIBUTION OF SECONDARY ELECTRONS

A. Derivation of the distribution

For an incident electron with energy E the total amount of energy deposited in ionization is

$$\int_{-\infty}^{\infty} D_{(e)}(x,E,\vec{e})dx = E \ , \tag{62}$$

and for an incident beam atom (or a target atom) with energy E,

$$\int_{-\infty}^{\infty} D_{(b)}(x,E,\vec{e})dx = \eta_{(b)}(E) \ . \tag{63}$$

$D(x,E,\vec{e})dx$ is the energy deposited in the depth interval $[x,x+dx]$ for all types of primary particles. The number of emitted electrons J with velocities in the interval $[\vec{v}_0, \vec{v}_0 + d\vec{v}_0]$ in the backward direction through the plane at $x=0$, initiated by a particle with velocity $\vec{v}$ at $x=0$, is found according to the treatment in Sec. II:

$$J(\vec{v}_0,\vec{v})d\vec{v}_0 = |v_{0x}|F(x,\vec{v}_0,\vec{v})d\vec{v}_0 \ . \tag{64}$$

Utilizing the result from Secs. V and VIII we may obtain the number J of electrons arriving at the plane $x=0$ in a backward direction from the value of the energy distributions, corresponding to Eqs. (62) or (63) at $x=0$:

$$J(E_0,\vec{e}_0,E,\vec{e})dE_0 d\vec{e}_0 = \Gamma_m \frac{D(0,E,\vec{e})|\cos\theta_0|}{NS_{e,e}(E_0)} \frac{dE_0}{E_0} \frac{d\vec{e}_0}{4\pi} \ . \tag{65}$$

Equation (65) states that the number of secondary electrons arriving at $x=0$ with energy E_0 in the direction $\vec{e}_0$ is proportional to the surface value of the energy distribution. The angular distribution is a cosine function because an isotropic approximation has been used for the zeroth-order moments. In fact, expression (65) is completely analogous to the corresponding sputtering formula.[46,73]

Until now the energy E_0 has been assumed high relative to the Fermi energy or the lowest level of the conduction band. An extrapolation of the expression (65) down to energies around the vacuum level seems now tempting. The band structure of the material may often be neglected since one deals with cascade electrons of energy larger than an eventual surface barrier. Even in the case of a single crystal of tungsten, for which the free electron model usually is insufficient, the band structure mostly results in a fine structure that is small compared to the background.[74] The particular density of states characterizing the medium enters the stopping power $NS_{e,e}(E_0)$ implicitly.

B. Inclusion of a surface barrier

So far the evaluation has been performed for an infinite medium. A real target, on the other hand, possesses a surface energy barrier and no stationary target nuclei or electrons will, of course, be present in the negative half space. The significance of eventual multiple crossing in an infinite medium will be discussed later in this section.

The standard model for the surface barrier is the work function model,[2,75] where energy E_1 and the direction $\vec{e}_1 = (\cos\theta_1, \sin\theta_1\cos\alpha_1, \sin\theta_1\sin\alpha_1)$ of the electron after passage through the surface barrier (Fig. 4) is connected to E_0 and $\vec{e}_0$ via[76]

$$E_1\cos^2\theta_1 = E_0\cos^2\theta_0 - U_0 \ , \tag{66a}$$

$$E_1\sin^2\theta_1 = E_0\sin^2\theta_0 \ , \tag{66b}$$

$$\alpha_1 = \alpha_0 \ . \tag{66c}$$

Substitution of

$$|\cos\theta_0|d\Omega_0 dE_0 = \frac{E_1}{U_0+E_1}|\cos\theta_1|d\Omega_1 dE_1 \tag{67}$$

in Eq. (65) yields the number of emitted electrons

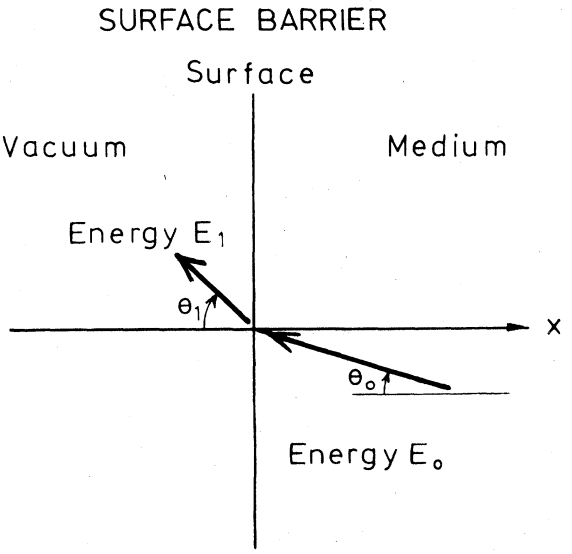

FIG. 4. Electron passing the surface barrier. For a planar barrier, described by Eq. (66), the energy component parallel to the surface remains unchanged.

through the surface, now expressed by the solid angle elements Ω_0 and Ω_1 and the variables E_1 and $\vec{e}_1$, as

$$J(E_1,\vec{e}_1,E,\vec{e})\,dE_1\,d\Omega_1 = \Gamma_m \frac{D(0,E,\vec{e})E_1 dE_1|\cos\theta_1|\,d\Omega_1}{NS_{e,e}(E_1+U_0)(E_1+U_0)^2 4\pi} \quad . \tag{68}$$

The total energy distribution is now obtained by means of an integration over $d\Omega_1$

$$J(E_1,E,\vec{e})\,dE_1 = \frac{\Gamma_m D(0,E,\vec{e})E_1 dE_1}{4NS_{e,e}(E_1+U_0)(E_1+U_0)^2} \quad . \tag{69}$$

This important result will now be discussed. We note immediately that Eqs. (68) and (69) account reasonably well for the behavior of known electron spectra. The spectrum will decrease to 0 as E_1 decreases to 0, and possesses a maximum, the position of which depends on the stopping power $NS_{e,e}(E_1 + U_0)$. For electron energies E_1 larger than the energy of the stopping power maximum the spectrum will decrease toward 0. The properties of the incident particle enter only into the surface value $D(0,E,\vec{e})$ of the energy distribution. For each type of primary particle one merely inserts the proper distribution for that particle.

The two spectra Eqs. (68) and (69) depend on the detailed behavior of the electronic stopping power $NS_{e,e}(E_1+U_0)$ for electrons in the energy region around $E_0 = U_0 + E_1$. The stopping power may again be utilized in the form (Table I) (here we set $m' = m$):

$$NS_{e,e}(E_1+U_0) = NC\frac{(E_1+U_0)^{1-2m}}{(1-m)} \quad , \tag{70}$$

so that m and thereby the slowly varying function Γ_m of m can be determined. In Table II, Γ_m is calculated for values of m in the interval $[-3,1]$.

For metal targets the surface barrier is determined by the work function ϕ and the Fermi energy E_F

$$U_0 = E_F + \phi \quad . \tag{71}$$

Both quantities may be found in standard tables.[77,78] For insulating materials the surface barrier corresponds to the electron affinity. The position of the maximum in the energy distribution Eq. (69) may be found. Assuming that the stopping power Eq. (70) is valid with the same exponent on both sides of the maximum, we find that the spectrum possesses its maximum at

$$E_1 = U_0/(2-2m) \quad . \tag{72}$$

The full width at half maximum $(\Delta E)_{1/2}$ of the energy distribution may be found from the same assumption. The corresponding equation is solved numerically, and $(\Delta E)_{1/2}$ is given in units of U_0 in Fig. 5 as a function of m in the exponent.

TABLE II. $\Gamma_m = m/[\psi(1)-\psi(1-m)]$, Eq. (38), as a function of m. Interpolations can be performed below $m = 0.6$ with an accuracy of 0.01.

m	Γ_m	m	Γ_m
−3.0	1.6364	−1.0	1.0000
−2.8	1.5775	−0.8	0.9279
−2.6	1.5179	−0.6	0.8532
−2.4	1.4574	−0.4	0.7755
−2.2	1.3959	−0.2	0.6940
−2.0	1.3333	0.0	0.6079
−1.8	1.2696	0.2	0.5157
−1.6	1.2046	0.4	0.4152
−1.4	1.1381	0.6	0.3024
−1.2	1.0700	0.7	0.2393
		0.8	0.1698
		0.9	0.0914
		1.0	0.0000

In order to verify the evaluated spectra and the characteristic quantities such as the position of the maximum and $(\Delta E)_{1/2}$ one requires the electron stopping power $NS_{e,e}(E_1+U_0)$ and m in the exponent of the corresponding approximation (70). For these energies ($\lesssim 20$ eV), which characterize most of the emitted secondary electrons, only few calculations exist. The low-energy stopping power of metals has been

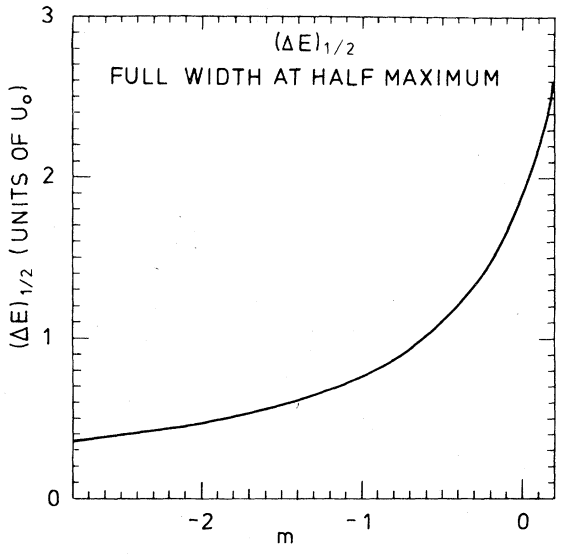

FIG. 5. Full width at half maximum $(\Delta E)_{1/2}$ of the secondary electron spectra plotted as a function of m in the electronic stopping power Eq. (70). $(\Delta E)_{1/2}$ is in units of the magnitude U_0 of the surface barrier.

calculated by Tung *et al.*[79,80] on the basis of a free electron model. Peterson *et al.*[81] have calculated the low-energy stopping power for electrons in some gases, but their evaluation is, of course, extended down only to the threshold for electronic ionization. One may then evaluate the distribution in relative units, while an absolute determination requires knowledge of the surface value $D(0,E,\vec{e})$ of the energy distribution. Some absolute comparisons will be given below.

The low-energy stopping power $NS_{e,e}(E_0)$ of aluminum as a function of the energy E_0 measured from the bottom of the conduction band is shown in Fig. 6. One notes that the stopping power for the lowest 10 eV above U_0 may be well approximated by a power function proportional to E_0^6 corresponding to $m=-2.5$. Also the experimentally extracted values of m, indicated below, yield examples of values of m below -1.

In the following a certain procedure will also be used for comparison with experimental data. The low-energy stopping power can be extracted from experimental spectra if Eqs. (68) and (69) are assumed valid for low E_1 up to a point around 10 eV above the vacuum level. Since the surface value $D(0,E,\vec{e})$ must remain unchanged, it is possible to determine the relative magnitude of $NS_{e,e}(E_1+U_0)$ as well as m in Eq. (70).

Finally it must be stated that the energy and angular distributions Eqs. (65) and (68) and the total energy distribution Eq. (69) all originate from an asymptotic expansion in E/E_0, and that they, therefore, cannot be expected to be accurate for ratios of E/E_0 which are too low.

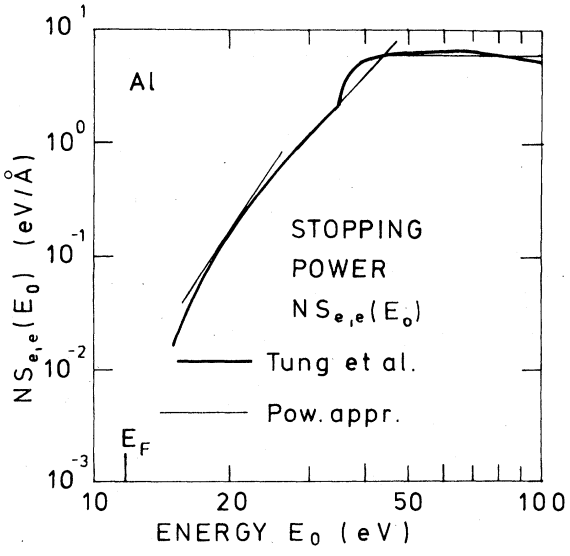

FIG. 6. Low-energy stopping power $NS_{e,e}(E_0)$ for electrons of energy E_0 (relative to the bottom of the conduction band) in aluminum from Ref. 80. The power approximations in Table IV are shown as well. E_F = Fermi energy.

C. Comparison with relative experimental data

Usually the secondary electron spectra, which may be found in the literature, are measured in relative units. With these we can test the agreement in shape; an absolute verification, however, is not possible.

For many years it has been accepted[2,5] that the position of the maximum of the secondary electron spectrum depends primarily on the surface barrier of the solid. Measurements of Wehner,[82] in particular, show that the maximum varies only a few tenths of one eV around the maximum at 2 eV over a factor of nearly 10 in the primary energy for noble gas ions bombarding molybdenum. Experiments on electron-induced spectra above 0.5 keV indicate[83–85] that the shape, the most probable energy, and the half width of the spectra are nearly independent of the primary energy in the energy range considered. Also, Musket[31] observed almost no difference below 50 eV between the energy spectra from incidence of 3-keV electrons on niobium and from incidence of 400-keV protons. These examples are in complete agreement with the predictions of Eqs. (68) and (69) which, apart from the surface value $D(0,E,\vec{e})$, are independent of the primary energy E and of the kind of primary particle.

Moreover, it was pointed out by Schaefer and Hölz[86] on the basis of experimental data that an increase of either the work function *or* the Fermi energy leads to an increase in the most probable energy *and* an increase of the half width. This connection is obviously demonstrated by Eq. (72) and Fig. 5, which states that the position of both the maximum and the half width are proportional to U_0. One notes that the total magnitude U_0 of the barrier rather than the Fermi energy or the work function is substantial in this respect.

The low-energy stopping power may, furthermore, be determined in relative units by Eq. (69) from experimental spectra, and following this, m is found. This has been done in Table III for five combinations of primary particle and target at widely different primary energies.[31,82,83,85,87] In all cases the surface barrier has been determined from other data.[77,78,88] One notes the agreement for the position of the maximum [Eq. (72)] and for the full width at half maximum (half width) based on the extracted m (Fig. 5) and the corresponding experimental quantities in nearly all cases.

The energy distribution Eq. (69) of the secondary electrons induced by primary keV electrons on aluminum has been calculated by means of the power approximation (Table IV) to the low-energy stopping

TABLE III. Comparison between the experimentally determined position of the maximum and the half width, and the corresponding calculated quantities from recent data for polycrystalline metals.

Authors and particle combination	Extracted m	Position of max. (eV) Expt.	Calc.	Half width $(\Delta E)_{1/2}$ (eV) Expt.	Calc.	Primary energy (keV)	$U_0 = E_F + \phi$ (eV)
Koshikawa and Shimizu (Ref. 85) $e^- \rightarrow$ Cu	−1.8	1.3	2.3	5.4	5.7	1.0	11.65 = 7.0 + 4.65
Louchet *et al.* (Ref. 87) $Ar^+ \rightarrow$ Cu	−1.35	2−3	2.5	7	7.3	60	11.65
Musket (Ref. 31) $H^+ \rightarrow$ Nb	−0.6	3	2.6	8	8.9	400	4.0 + 4.3 = 8.3
Wehner (Ref. 82) $He^+ \rightarrow$ Mo	−1.1	1.9	2.0	5.4	6.2	15	4.0 + 4.6 =8.6
Everhart *et al.* (Ref. 83) $e^- \rightarrow$ Al	−2.7	1.5	2.1	8.9	5.8	1.0	15.6 = 11.6 + 4.0

power. One notes the agreement between the theoretical distribution and the experimental data of Everhart *et al.*[83] and Bindi *et al.*[89] in Fig. 7. Also a spectrum recorded on a (421) surface of a single crystal[84] has been included.

D. Comparison with absolute experimental data

A fair agreement has been obtained between the experimental data of Combecher *et al.*[90] and the theoretical energy and angular distribution Eq. (68).[41]

TABLE IV. Power approximations $[NC/(1-m)]E_0^{1-2m}$, Eq. (70), to the electronic stopping power $NS_{e,e}(E_0)$ in aluminum on the basis of the calculations of Tung *et al.* (Ref. 80).

Energy interval	NC $[(\text{eV})^{2m}\text{Å}^{-1}]$	m
E_0: [15.6, 25.6] E_1: [0.0, 10.0]	2.75×10^{-9}	−2.5
E_0: [25.6, 46.3] E_1: [10.0, 30.7]	8.56×10^{-7}	−1.59
E_0: [46.3, 65.6] E_1: [30.7, 50.0]	4.26	0.50

Combecher *et al.*[90] measured the energy and angular distribution from a carbon foil of thickness around 3.7 $\mu g/cm^2$ for perpendicular incidence of 1-keV electrons. In Ref. 41 two existing calculations of the low-energy stopping power $NS_{e,e}(E_0)$ were used.

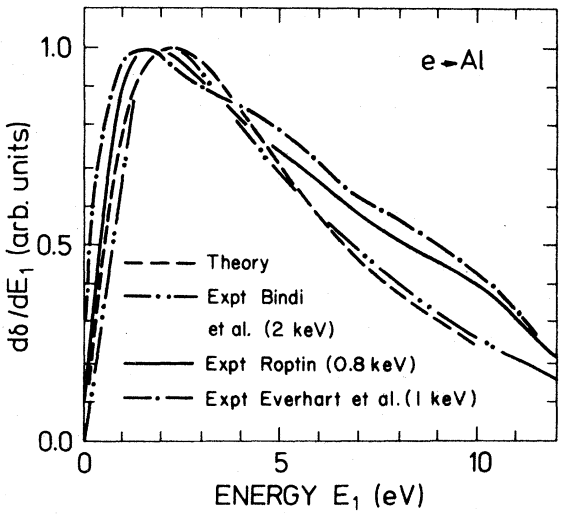

FIG. 7. Energy spectrum $(d\delta/dE_1)$ of the secondary electrons for perpendicular incidence of 0.8- , 1- , and 2-keV electrons on aluminum. Experimental results: (——·——), Ref. 83; (——), Ref. 84; (——··——), Ref. 89; (– – –), theoretical curve for $J(E_1, E, \vec{e}_x)$, Eq. (69). A surface barrier model Eq. (66) with $U_0 = 15.6$ eV has been used.

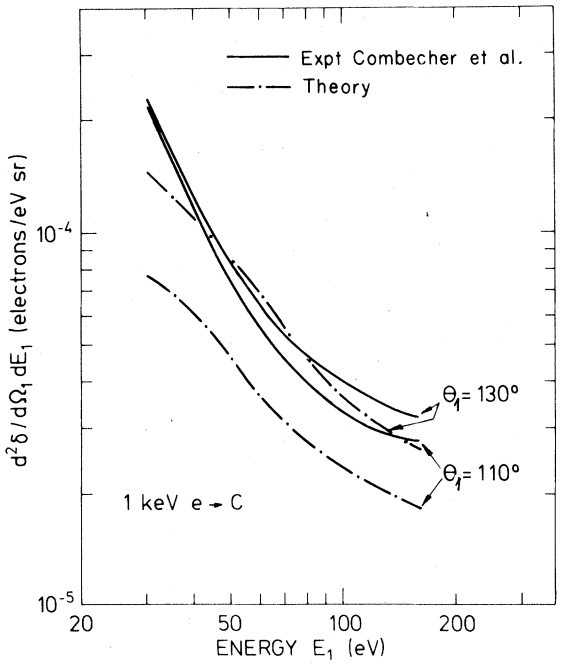

FIG. 8. Energy and angular spectrum $(d^2\delta/d\Omega_1 dE_1)$ for normal incidence of 1-keV electrons on a carbon foil at the deflection angles $\theta_1 = 110°$ and 130°. (——), smoothed experimental results (foil 2), Ref. 90; (– –), theoretical curves, Eq. (68), with a surface barrier model Eq. (66) with $E_F = 17.3$ eV and $\phi = 5.0$ eV, with $\beta = \frac{3}{4}$, Eq. (79), and with low-energy stopping power $NS_{e,e}(E_0)$ from Ref. 81.

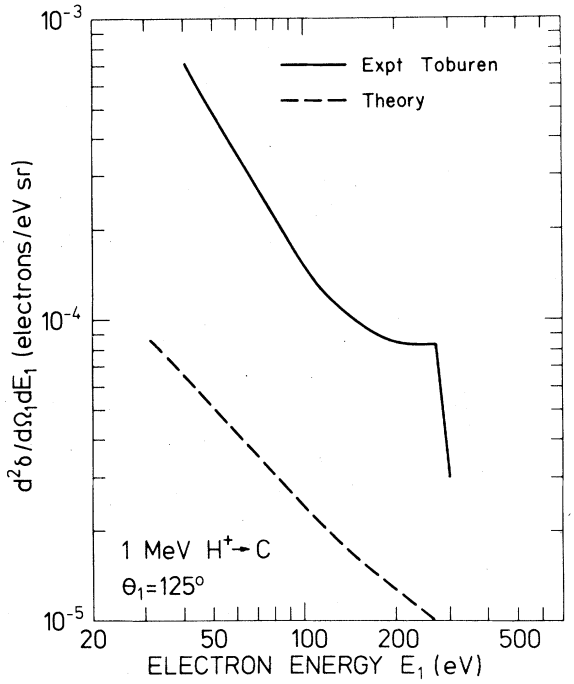

FIG. 9. Energy and angular spectrum $(d^2\delta/d\Omega_1 dE_1)$ for normal incidence of 1-MeV protons on a carbon foil at a deflection angle $\theta_1 = 125°$. (——), experimental results, Ref. 92. (– – –), theoretical curve, Eq. (68), with $\beta = \frac{1}{4}$, Eq. (79), and with surface barrier and low-energy stopping power as in Fig. 8.

However, since the stopping power[79] based on the free-electron model[91] corresponding to a Fermi energy of 17.3 eV yielded a theoretical curve of more than a factor of 2 below the experimental results, use here will be made of the stopping power of Peterson and Green[81] only. Their stopping power of nitrogen has been applied directly, because a comparison with the corresponding low-energy stopping power of oxygen indicates that it is rather insensitive to small changes in Z_2 at these energies. In Fig. 8 the calculation based on the theoretical expression, Eq. (68), has been compared to the experimental results at deflection angles $\theta_1 = 110°$ and 130°. One notes that the absolute agreement is satisfactory, and that the theoretical curves show a similar trend with respect to dependence on θ_1 and E_1 as do the experimental data. According to the discussion in Sec. X C the surface value of the deposited energy in Eq. (68) is estimated to the stopping power for the primary $NS_e(E)$ multiplied with a factor $\beta = \frac{3}{4}$. β accounts for the amount of the dissipated energy that is available for secondary electron emission at the surface.

Recently Toburen[92] performed absolute measurements on carbon foil of thickness 20 μg/cm^2 for perpendicular incidence of 1-MeV protons at several deflection angles. The theoretical energy distribution at $\theta_1 = 125°$ lies, unfortunately, at least a factor of 5 below the experimental curve (Fig. 9), but the dependence on E_1 is relatively well predicted by theory (apart from the Auger peak around $E_1 = 270$ eV, which is disregarded). Here the low-energy stopping power of nitrogen[81] and a surface value equal to $\frac{1}{4} NS_e(E)$ (cf. Sec. X C) was used, while the proton stopping power was taken from Ref. 93.

The comparative analyses have been performed for electron energies larger than 30–40 eV, since energies in this range are less sensitive to surface contamination which otherwise may change the spectrum considerably. On the other hand, the energy and angular distribution Eq. (68) is, as mentioned above, most accurate for large ratios of E/E_0. In both cases the thickness of the foil is comparable to the range of the primaries or of the most energetic recoil electrons,[94] so that the cascade can develop almost as in a semi-infinite solid. Finally, the atomic density N does not influence the spectrum Eq. (68), as the density in the denominator cancels the density in the surface value of the deposited energy. In view of the relatively uncertain low-energy stopping power the absolute agreement with the data of Combecher *et al.* is acceptable, whereas the agreement with the proton data is less satisfactory.[95]

E. Corrections due to binding energy at ionization

In this treatment we have until now neglected the electron's binding energy at its liberation. This may be used as an approximation for metals, where we often expect the excitation of conduction electrons to be important. For bound electrons in insulators the energy loss at the ionization may be considerably larger than the surface barrier energy U_0. Thus by including binding energy V at the ionization the energy spectrum should be modified. For convenience we consider the binding energy as being independent of the emitted angle. In Eq. (14) we set

$$E' = E - T, \quad E'' = T - V \ . \tag{73}$$

The spectrum may now be evaluated by a procedure developed by Sigmund[46] and described by Andersen and Sigmund,[96] and one obtains for the energy and angular distribution Eq. (65)

$$J(E_0, \vec{e}_0, E, \vec{e})\, dE_0 d\Omega_0 \approx \frac{\Gamma_m D(0, E, \vec{e})\, dE_0}{N S_{e,e}(E_0)[E_0 + (2-m)V]} \frac{d\Omega_0}{4\pi} \ . \tag{74}$$

Independent of the precise value of the exponent m, one notices that the correction relative to Eq. (65) in Eq. (74) becomes more important with decreasing energy E_0. The inclusion of a surface barrier with the conditions (66) and the binding energy in the distributions Eqs. (68) and (69) means that one of the factors $(E_0 + U_0)$ in the denominator is replaced by $[E_1 + U_0 + (2-m)V]$.

Equation (74) leads to an important result with regard to the origin of secondary electrons. The contribution from the different shells of the target atoms to both the spectrum and total yield decreases with rising binding energy. Thus in metals the liberated electrons originate mostly from the conduction band.

F. Energy spectra for transmitted beams

Let us suppose the target has a finite thickness d. In the infinite medium we may then consider the secondary current at the entrance plane $x = 0$ and the forward secondary current through the plane $x = d$. Similar to transmission sputtering we find the number of electrons per incident particle passing the plane $x = d$ in forward direction:

$$J(E_0, \vec{e}_0, E, \vec{e})\, dE_0 d\Omega_0 = \frac{\Gamma_m D(d, E, \vec{e})}{N S_{e,e}(E_0)} \frac{dE_0}{E_0} \cos\theta_0 \frac{d\Omega_0}{4\pi} \ . \tag{75}$$

One notices that the energy distributions Eqs. (65) and (75), apart from the absolute magnitude are identical.

In the forward direction around $\theta_1 = 50°$, Toburen[92] recorded the electron energy spectra at the same conditions as for backward emission. The spectrum in the forward direction from $E_1 = 50$ eV up to 250 eV is actually a factor of 2.3 larger than the spectrum in the backward direction around $\theta_1 = 125°$, but has almost the same shape in this energy interval. This means that the ratio of the surface values $D(d, E, \vec{e}_x)/D(0, E, \vec{e}_x)$ is approximately 2.1 ($\vec{e}_x$ is the unit vector along the x axis). Since there is no significant multiple scattering for 1-MeV protons through a 20 $\mu g/cm^2$ carbon foil, and since the stopping power for the proton is almost unchanged through the foil, the increase of the surface value in the forward direction must be caused by fast recoil electrons. This will be further discussed in Secs. X and XI.

G. Corrections for multiple crossings of the surface

Until now the evaluation of the distributions Eqs. (65), (68), and (69) has been performed in an infinite medium with the eventual inclusion of a surface barrier. Corrections caused by the possible scattering forth and back through the surface of the solid in the theoretical evaluation will not be applied quantitatively.

Multiple crossings in the infinite medium may occur for the secondary electrons, the primary particles, or the target atoms which are possibly set in motion. These corrections become important with increasing angles with respect to the surface normal at the crossings.[73] A correction for (low-energy) *secondary* particles has been derived in Ref. 73 including a correction for multiple crossings by primary particles within the isotropic approximation.

In the present work these corrections will be disregarded. For the most part we shall consider perpendicular incidence, where the correction for multiple crossings of the primaries is minor. Furthermore, the contribution from recoiling target atoms is important only for heavy-particle incidence at some particular energy regions (cf. Sec. XII). The angular distribution of these particles is peaked in a rather forward direction. Finally, one notes that the energy distribution Eq. (69) is peaked at a few eV above the vacuum level $E_1 = 0$. Hence, the majority of the emitted (secondary) electrons will be slowed down by electronic stopping to a level below the surface barrier after two surface crossings.

X. YIELD OF SECONDARY ELECTRONS

A. Yield formula

The total yield may be evaluated by means of the results of the previous section. We consider both the case of incident electrons and atomic ions. Let us in-

troduce a material parameter

$$\Lambda = \int\int_{E_0 \geq U(\cos\theta_0)} \frac{\Gamma_m |\cos\theta_0| dE_0 d\Omega_0}{NS_{e,e}(E_0) E_0 4\pi} \quad . \tag{76}$$

Here a planar surface barrier $U(\cos\theta_0)$, depending on the directional cosine of the emerging electron, was assumed. The total yield δ is now determined by the basic relation,

$$\delta = D(0,E,\vec{e})\Lambda \quad . \tag{77}$$

The properties of the primary particle enter only through the surface value $D(0,E,\vec{e})$ of the deposited energy. Equation (77) holds only for energies E high enough so that the angular distribution of the ejected secondaries is a cosine distribution.

For electron incidence the concept true secondary electrons is used for the emitted electrons up to 50 eV. The precise position of the upper limit is quite arbitrary, and in the following we shall use some energy E_u as the upper limit. If the stopping power Eq. (70) remains valid with the *same* value of the exponent in the interval $[0,E_u]$ and if the surface barrier Eq. (66) is applied, we obtain for the material parameter,

$$\Lambda = \frac{\Gamma_m}{8(1-m)(1-2m)NS_{e,e}(U_0)} \times \left[1 - \frac{2(1-m)}{(E_u/U_0+1)^{1-2m}} + \frac{(1-2m)}{(E_u/U_0+1)^{2-2m}}\right] \tag{78}$$

for $E >> E_u$.

For $E_u/U_0 >> 1$ and $m = 0$ the total yield δ will be given in a form analogous to the sputtering yield formula.[33] Naturally, in Eq. (78) we deal with the surface value of the distribution of energy delivered to the electrons, $D(0,E,\vec{e})$, rather than the distribution of energy deposited in atomic motion, which enters in sputtering. Moreover, for sputtering the relevant energy loss property in the denominator is the nuclear stopping power $NS_{t,t}(U_0)$ of the emerging target atoms, and U_0 is the sublimation energy rather than the magnitude of the surface barrier. One notes that the yield is determined by three quantities, the energy deposited in the surface, the surface barrier energy U_0, and the electronic stopping power $NS_{e,e}(U_0)$ of the electrons at the energy U_0. The value of m is governed by the exponent in the electronic stopping power in the energy region above $E_0 = U_0$.

B. Connection between the electronic stopping power and the surface value of D

It appears desirable to find the connection between the electronic stopping power $NS_e(E)$ for the primary particle and the surface value of the deposited energy. By a dimensional arguement we can express

$$D(0,E,\vec{e}) = \beta NS_e(E) \tag{79}$$

with the dimensionless function $\beta(E,\vec{e})$. This definition becomes particularly useful when recoiling target atoms do not play an essential role in the generation of secondary electrons. The opposite situation is studied in Sec. XII and in Ref. 42. Thus β is utilized mainly for light primary particles, electrons or protons, or for heavier particles in the energy region where nuclear stopping is of minor importance compared with electronic stopping. Generally β needs to be evaluated by means of transport theory, and this is done in Sec. X C below.

It turns out in the following that β is a very slowly varying function of the primary energy, but strongly dependent on the type of particle and the angle of incidence. The analog to β in sputtering theory is the factor α,[33,40] which will be denoted here by α_D. For light beam particles on heavy targets backscattered primaries may also deposit energy in the surface on

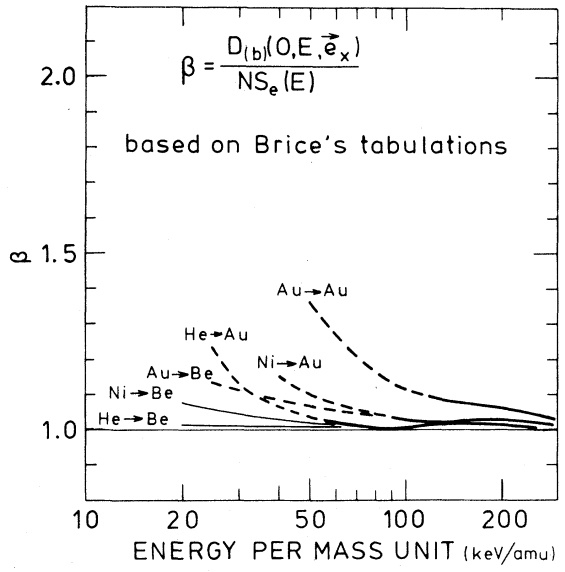

FIG. 10. Factor $\beta = D_{(b)}(0,E,\vec{e}_x)/NS_e(E)$, Eq. (79), for six different beam-target combinations. β is plotted as a function of the energy per mass unit, and calculated on the basis of Brice's tabulations (Ref. 38). (——), β for the reduced energy ϵ, Eq. (22), $\epsilon \geq 10$; (– – –), β for $\epsilon \leq 10$. The electronic stopping power $NS_e(E)$ for a beam ion is taken from the same reference. The correction for energy transport by recoil electrons is *not* included. The limit $\beta = 1$ is also shown.

their way out, thereby giving rise to larger values of β. For primary electrons it has already been pointed out in Sec. VI A that β_{unc} indeed is almost insensitive to variations of the primary energy E.

For incident ions the factor β can be evaluated from Brice's tabulations.[38] β has been depicted as a function of the energy per mass unit for six representative beam ion-target combinations in Fig. 10. For values of the reduced energy ϵ [Eq. (22)] larger than 10 the factor β changes obviously less than 10% in the depicted energy region from 20 keV/amu and beyond.

With the notation Eq. (79) the yield may be expressed as

$$\delta = \beta N S_e(E) \Lambda \ . \tag{80}$$

Apart from the slow variation of β with the energy, δ is proportional to the electronic stopping power. This approximate proportionality (without inclusion of the factor β) has experimentally been recognized by numerous authors already.[28, 31, 32, 97–99]

C. Surface corrections to β

In the discussion of β, the influence of recoiling electrons has been mostly neglected. The energetic recoiling electrons may transport energy over distances comparable to their range. However, this energy transport does not affect the profile of the deposited energy in the interior of the medium. The energy that is carried away initially from a certain depth by fast recoiling electrons is obviously replaced by the energy delivered by recoiling electrons originating from other depths according to the discussion in Secs. VIII C and VIII D. Corrections will therefore be necessary only at the surface, i.e., the plane where the primary particles start to dissipate energy or where the outgoing particles finish their energy dissipation.

It is clear from the general shape of the distribution $D_{(e)}$ (Fig. 3) that on the average a recoiling electron deposits more energy in its forward (initial) direction, from the point where it was liberated, than in its backward direction. A schematic example of a distribution $D_{(b)}$, which has been corrected for energy transport by recoiling electrons, is shown in Fig. 11. The primary ion penetrates a medium of thickness d essentially undeflected and with only a small relative energy loss. On the other hand d is much larger than the range of the most energetic recoiling electrons. One notes that the deposited energy at $x=0$ is considerably less than the stopping power, since most of the energetic recoiling electrons have a direction into the medium. This results in an energy transport towards larger depths. At the exit $x=d$ the value of the deposited energy almost reaches the value of the stopping power, because only the minor contribution from recoiling electrons from depths

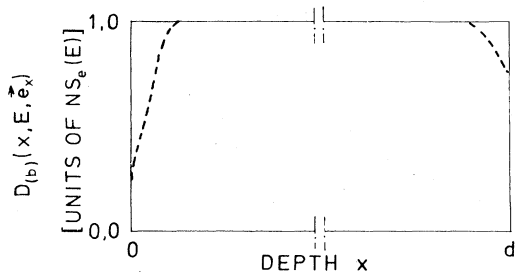

FIG. 11. Energy distribution $D_{(b)}(x,E,\vec{e}_x)$ for a foil of thickness d. The energy transport by recoiling electrons is included. The primary ion is assumed to penetrate the foil perpendicular to the surface without scattering or energy loss, whereas d is assumed large relative to the range of the most energetic recoiling electrons.

larger than d vanishes. These corrections occur for all primary particles; the smearing out of the profile around $x=0$ at electron bombardment has been demonstrated experimentally by Grün[60] and Cohn and Caledonia.[61]

β can be directly determined by a procedure described in Ref. 33. For perpendicular incidence ($\vec{e}=\vec{e}_x$) of a beam ion, one finds, as indicated in Ref. 45 by means of a power cross section with an exponent m for a beam atom-electron collision, that

$$\beta_0 = \left[\frac{1}{2} + (1-m)\left(\frac{2m-5}{2(3-2m)(2-m)} + \frac{k_p(\gamma E)^{-p}(5-2m-2p)}{(3-2m-2p)(2-m-p)}\right)\right] , \tag{81}$$

where

$$k_p E^{-p} = \frac{1}{E}\int_0^\infty dx D_{(e)}(-x,E,\vec{e}_x) \tag{82}$$

is a power approximation to the fraction of energy that is reflected (in an infinite medium) at perpendicular electron incidence. $\gamma = 4m_e/M_1$. For Rutherford scattering $\beta_0 = \frac{1}{2}$, which is entirely analogous to the corresponding value in sputtering.[33] One notes that β_0 is, indeed, a slowly varying function of the energy, because m, as discussed in Sec. IV, varies slowly with the energy. The inclusion of energy transport does not change the fact, then, that for primary ions with $\epsilon \geq 10$ as shown above, β is rather insensitive to variations in the primary energy.

The fraction of reflected energy can be found from extrapolations from Spencer,[64] Grün,[60] or Cohn and Caledonia.[61] It is also possible to use experimental values[100] (from semi-infinite media), because β_0 is only moderately sensitive to changes in $k_p E^{-p}$, e.g., due to differences between the value for a semi-infinite and an infinite medium. Then the power approximation to the fraction of reflected energy may

be determined from the expression of Bronshtein and Stozharov[100] at two values of the primary electron energy E:

$$k_p E^{-p} \approx \begin{cases} 0.6\eta(E) \text{ for } E = 0.2 \text{ keV}, & \text{(83a)} \\ (0.31 + 0.0025 Z_2)\eta(E) \text{ for } E = 1 \text{ keV}. & \text{(83b)} \end{cases}$$

The number $\eta(E)$ of reflected electrons with energy larger than 50 eV per incident electron can be taken from recent measurements. Also Spencer's tabulation[64] may yield a value of $k_p E^{-p}$, since $k_p E^{-p}$ generally varies slowly with the energy.

The factor β obviously depends on the angle of incidence θ. The corresponding factor α_D has been evaluated as a function of the angle of incidence in sputtering theory,[33] and it shows a variation somewhat stronger than a $1/\cos\theta$ so long as the exponent m in the cross section is below 1.

The corresponding surface value for an emergent particle, e.g., at transmission or reflection, is found by multiplying the stopping power $NS_e(E)$ with $(1-\beta_0)$ where β_0 is determined from the case where the same kind of particle enters the layer in the opposite direction. Generally β, Eq. (80), should be evaluated on the basis of the complete energy and angular distribution of the reflected primaries and of the recoiling target particles.

For electron incidence the corrected surface value can be found by a crude estimate. Let us assume that all reflected electrons pass out through the surface layer perpendicular to the surface and still possess the primary energy E. If the uncorrected value β_{unc} is available, e.g., from Spencer's tabulations,[64] we obtain by means of the directly obtained β_0 Eq. (81) for the total β:

$$\beta = \beta_0 + (\beta_{\text{unc}} - 1)(1 - \beta_0) \approx \tfrac{1}{2}\beta_{\text{unc}} \ ; \qquad \text{(84)}$$

here β_0 is taken to be approximately $\frac{1}{2}$, since the primary electron energies are in the keV region. By means of Eq. (84) one finds from an average over the existing data for β_{unc}[60,62,67] that $\beta \approx \frac{3}{4}$ for the data of Combecher *et al.*, Fig. 8.

The accuracy of the approximations leading to Eq. (81) may be tested to the extent that double differential cross sections for electron ejection at primary collision processes exist. From data for 1 MeV proton incidence on several gaseous hydrocarbons[101] one finds by numerical integration that $\beta = 0.245$ for 1-MeV protons on carbon. The formula (81) yields a corresponding value $\beta = \beta_0 = 0.21$ from $m = 0.85$ as determined from the stopping-power tabulations.[93] In both cases an approximation (82) with $k_p = 0.075$ (E in keV) and $p = 0.324$, obtained by extrapolation with respect to Z_2 of data for air,[68,102] has been used. The agreement between the two values of β is satisfactory. It is, therefore, possible to utilize $\beta = \beta_0$, so long as the real cross sections from the primary collision processes do not deviate too much from the corresponding power cross sections.

D. Evaluation of the secondary electron yield from aluminum

The material parameter Λ Eq. (78) may be evaluated by means of the calculated stopping power $NS_{e,e}(E_0)$ of aluminum.[80] By means of three power approximations, given in Table IV, the material parameter is determined to $\Lambda = 0.29$ Å/eV for electron energies up to $E_u = 50$ eV. Here the surface barrier had the value $U_0 = 15.6$ eV.

For *electron-induced yields* Spencer's tabulations[64] lead to $\beta_{\text{unc}} \approx 2$, corresponding to a value $\beta = 1$ in Eq. (80) according to Eq. (84). Utilizing the stopping power $NS_e(E)$ from Tung *et al.*[80] one obtains striking absolute agreement[41] with experimental data at primary energies from 1 to 4 keV.[84,103,104]

For proton-induced yields at primary energies around the maximum for the electronic stopping power (40 to 70 keV) one estimates with $m = \frac{1}{2}$ and $k_p E^{-p} = 0.15$ the corresponding value $\beta = \beta_0 = 0.27$ from Eq. (81). The energy fraction $k_p E^{-p}$ has been determined from secondary electron emission data.[103] By means of Eq. (80) this leads to a secondary electron yield $\delta = 0.077\ NS_e(E)$ (with NS in eV/Å) around the stopping-power maximum. This expression gives a fair agreement[41] with experimental data,[97,105] when the stopping-power tabulations[93] are used.

The calculations of the low-energy stopping power has recently been refined by Ashley *et al.*,[53] who demonstrated that various improvements may lead to a change in the magnitude up to a factor of 1.3. The agreement with experimental data for the theoretical inverse mean free path within the electron gas model is, however, satisfactory down to the lowest experimental energies around $E_1 = 5$ eV.

The stopping power utilized here does not include a correction for exchange. Tung *et al.*[80] have introduced a semiempirical correction for exchange in their stopping power, and this stopping power leads to an increase of 30% in the material parameter by using the modified power cross section in Ref. 45. These exchange corrections are, however, rather uncertain for energies E_0 around U_0.

The contribution from plasmons is partly included. The energy loss at plasmon generation enters into the surface value of the deposited energy (by entering the stopping power for the primary). On the other hand the particular features pertaining to excited plasmons are disregarded to the extent that the number of liberated electrons generated by an excited plasmon deviates from the corresponding number

generated by an energetic electron. Of course, changes in the model cross section (Table I) and in the collision parameters (Sec. III) from an electron-electron collision to an electron-plasmon (or plasmon-electron) collision in the analytical procedure are neglected as well. However, according to Lindhard's equipartition rule[106] the plasmon contribution to the stopping power is always less than the contribution of single particle excitation. Consequently the contribution from plasmon decay to the total yield should also be less than the contribution from excitation of free electrons. In view of this the present treatment seems adequate. One should note that it has occasionally been asserted that the plasmon contribution is a dominant factor in secondary electron emission.[107,108]

E. Comparisons with experimental data

As low-energy stopping powers $NS_{e,e}(E_0)$ are somewhat uncertain, a test of the theoretical predictions can be performed as follows: from the knowledge of the values of the secondary electron yield, the electronic stopping power and eventually, the factor β, an experimental material parameter $\delta_{\text{expt}}/D(0,E,\vec{e})$ can be extracted according to Eq. (80). For different primary particles on the same target material, one expects comparable extracted material parameters.[42] For a direct test of the theoretical predictions secondary electron emission data for different incident particles on the same target at similar experimental conditions should be available. Also the corresponding stopping power $NS_e(E)$ should be known sufficiently accurately for those cases. Unfortunately, such measurements are rare.

Let us compare the experimental data on copper with the theoretical predictions. Unfortunately, electron bombardment and proton bombardment of copper have not been studied under the same experimental conditions. Koshikawa and Shimizu[85] measured the secondary electron emission coefficient for electron incidence at primary energies up to 10 keV. From Spencer's tabulations[64] and Eq. (84) the estimate is $\beta=1.5$. One then obtains an extracted material parameter around 0.083 Å/eV by means of Bethe's stopping-power expression. For proton incidence at 400 keV ($m=\frac{2}{3}$) one finds with $\beta=\beta_0=0.31$ from the data of Holmén *et al.*[98] a material parameter of 0.28 Å/eV. Near the stopping maximum ($m=\frac{1}{2}$) one obtains with $\beta=0.27$ a material parameter of 0.30 Å/eV. For incidence of 100-keV helium ions ($m=\frac{1}{4}$), one finds a material parameter of 0.23 Å/eV. Here the stopping power expression of Lindhard and Scharff[54] has been utilized. For larger helium ion energies the material parameter decreases somewhat. The parameters for copper are listed in Table V.

The agreement between the material parameters from electron and proton incidence is not satisfactory, but the agreement between the parameters from helium ion and proton bombardment is as expected. It is noteworthy, however, that the data for electron incidence of Koshikawa and Shimizu are approximately 30% lower than the somewhat older data of Bronshtein and Fraiman.[109]

F. Comparison with existing theories

Before comparing the present results with Sternglass's theory[14] and that of Parilis and Kishinevsky,[24]

TABLE V. Extracted experimental material parameters $\delta/D(0,E,\vec{e}_x)$, cf. Eq. 77, for several beam particles on a copper target. For ion incidence $k_pE^{-p}=0.15$ has been utilized (Ref. 103). The yield from incident inert gas ions has not been corrected for potential emission.

Author	Beam particle	Primary energy (keV)	Extracted experimental material parameter: $\delta/D(0,E,\vec{e}_x)$ (Å/eV)
Koshikawa and Shimizu (Ref. 85)	e^-	10	0.083
Bronshtein and Fraiman (Ref. 109)	e^-	4	0.15
Holmén *et al.* (Ref. 98)	H^+	400	0.31
	He^+	100	0.23
	Kr^+	204	0.13
	Xe^+	219	0.09

we shall summarize the existing semiempirical theories. Generally[1,27] the yield is written in the form:

$$\delta = \int_0^\infty n(x,E) f(x)\, dx \quad , \tag{85}$$

where $n(x,E)\,dx$ represents the average number of secondaries produced per incident electron in a layer of thickness dx and depth x. The probability for a secondary to migrate and escape from the surface is represented by $f(x)$. Normally,[1,14,27] it is assumed that $n(x,E)$ is proportional to the electronic stopping power $NS_e(E)$. Furthermore, one can assume that the electrons originate mainly from an escape zone of depth λ near the surface. Thus one obtains the following approximate expression:

$$\delta = \frac{1}{\epsilon_0} \int_0^\lambda NS_e(E^*(x)) f(x)\, dx \quad , \tag{86}$$

where ϵ_0 is the average energy required to produce a secondary electron, and $E^*(x)$ is the average energy of the *primaries* as a function of depth. Through a thin escape zone the stopping power may be regarded as a constant of value $NS_e(E)$, and

$$\delta = NS_e(E) \left(\frac{1}{\epsilon_0} \int_0^\lambda f(x)\, dx \right) \tag{87}$$

is obtained.

The escape integral is often written in a more complicated way but uncertain points remain such as the value of the constant of proportionality ϵ_0 and the omission of any scattering of the primaries. In the case of electron bombardment a clear distinction between the reflected primaries and the (true) secondaries is not always emphasized in semiempirical treatments. Furthermore, $n(x,E)$ is proportional only to $NS_e(E^*(x))$ with the *same* constant of proportionality, so long as the energetic recoil electrons that transport energy away from the surface (as pointed out in Sec. X C) are neglected. The semiempirical treatment has often been utilized, since it demonstrated the observed proportionality between yield and stopping power.

The semiempirical yield Eq. (87) is, to some extent, similar to the yield formulas (77) and (80). The material parameter in the latter formulas may be calculated from the knowledge of the low-energy-electron stopping power, while the semiempirical material parameter, indicated by the parentheses, is evaluated from data of ionization in gases, or from the knowledge of properties in solid state physics. A critical discussion of some theories for ion-induced emission has recently been given in Ref. 110.

In the theory of Sternglass[14] the yield is written

$$\delta = \tfrac{1}{2}[1 + f_s(E)] NS_e(E) \left(\frac{1}{\epsilon_0} k_s L_s \right) \tag{88}$$

in the present notation. The factor $\frac{1}{2}[1 + f_s(E)]$ corresponds to β in the Rutherford region ($m = 1$) with an additional correction $f_s(E)$ for the contribution of reflected energetic recoil electrons to the surface value of the deposited energy. The energy ϵ_0 required to liberate an electron was taken from known values of the average energy for an ionization in a gas. The constant k_s was determined as the product of the transmission probability through the surface and a constant characterized by the initial velocity distribution of the liberated electrons. Finally, L_s was a characteristic diffusion length with respect to inelastic collisions for these electrons. Sternglass chose fixed values, $\epsilon_0 = 25$ eV and $k_s = 0.5$, for all metals, whereas L_s was determined on the basis of a geometric area of the outermost filled shells.

The energy dependence and the absolute magnitude of the yield were in good agreement with the existing data. These data are, however, around a factor of 2 larger than recent data in which surface conditions were controlled.[98,110] Moreover, Sternglass did not include in his theory any correction for scattered primaries or recoiling target atoms.

On the basis of Auger recombination Parilis and Kishinevsky[24,25] formulated a theory covering the energies in the lower part of the energy region, where the electronic stopping power is proportional to the velocity. Only metal targets are considered, and the yield is written as

$$\delta = N \sigma^*(E) \lambda w(\tau) \tag{89}$$

in the present notation. Here the effective ionization cross section $\sigma^*(E)$ was evaluated from the excitation cross section by Firsov.[111] $w(\tau)$ is probability of extracting an electron as the result of an Auger process, including the probability of passing the surface barrier, and τ is the energy of the band in which the corresponding hole is located.

The energy dependence of the yield is explained by the energy dependence of the effective cross section $\sigma^*(E)$, which for primary energies around 0.1–0.2 keV/amu, is proportional to the energy, and for energies somewhat larger is proportional to the velocity. $w(\tau)$ was based on an expression from potential emission and on Auger emission data from molybdenum and tungsten. The agreement with data for these two metals was good, but, unfortunately, the basic input quantities, the escape depth λ, the band depth τ, and an ionization potential in $\sigma^*(E)$, are not usually directly available.

The theory by Parilis and Kishinevsky concerns low primary energies, which are expected to be covered only partly by the present treatment. On the other hand their theory does not include contributions from recoiling target atoms, and this is a substantial deficiency in their theory, which was later rectified.[112]

XI. CORRECTIONS AT TRANSMISSION

Let us regard in more detail the surface correction caused by the interruption of the energy dissipation (cf. Sec. X C). The ratio between the surface values for primary ions which penetrate a foil of thickness d without scattering and energy loss (Fig. 11), is determined by

$$\frac{D_{(b)}(d,E,\vec{e})}{D_{(b)}(0,E,\vec{e})}=\frac{1-\beta}{\beta} \quad . \tag{90}$$

This simple relation does not hold under conditions where the primaries are scattered considerably, e.g., electrons passing a foil so thick that a cascade largely may develop.

Equation (90) yields for 1-MeV protons on carbon with the value $\beta=0.245$ from Sec. IX C a ratio of 3.1 compared with the ratio 2.1 deduced from the experimental data in Sec. IX F.

XII. CONTRIBUTION TO THE YIELD FROM RECOILING ATOMS

A. Influence of recoiling target atoms

In Sec. X the yield dependence on energy for light ions was discussed, and it was pointed out that the yield was nearly proportional to $E^{1/2}$ below the maximum for the electronic stopping power according to Eq. (80). A different behavior has, however, been observed experimentally for bombarding heavy ions,[98] and it was pointed out[98,113] that recoiling target atoms might contribute substantially to the secondary electron yield at heavy ion incidence.

Obviously, the recoiling target atoms are important if a considerable fraction of the primary energy is delivered to the electrons by these target atoms. Of course, the nuclear stopping power must be so large that an appreciable number of fast recoils are set in motion. For a fixed target and a fixed primary velocity the largest recoil velocities are obtained for small mass ratios M_2/M_1. Furthermore, the electronic stopping power is proportional to the velocity by a factor which increases with decreasing mass ratio. Hence, the contribution from recoiling atoms is most significant for small mass ratios M_2/M_1. It turns out that the energy distribution $D_{(b)}$ can be divided conveniently into two separate distributions, of which the first, $D_{(p)}$, represents the energy lost directly to the target electrons by the $p$rimaries including recoil electrons. The second, $D_{(r)}$, represents the energy deposited by $r$ecoiling target atoms with eventual recoil electrons. The feasibility of this separation is convincingly demonstrated by recent measurements of the yield dependence on the angle of incidence.[114] The treatment given here extends the derivation by Holmén *et al.*[42]

B. Separation of the distribution $D_{(b)}$

The energy distribution $D_{(b)}$, described in Secs. VII and VIII, may be expressed as

$$D_{(b)}(x,E,\vec{e})=D_{(p)}(x,E,\vec{e})+D_{(r)}(x,E,\vec{e}) \quad . \tag{91}$$

This relationship is, of course, also valid for the corresponding zeroth-order moments $\eta_{(b)}$, $\eta_{(p)}$, and $\eta_{(r)}$.

The distributions $D_{(p)}$ and $D_{(r)}$ each obey the transport equations given in Ref. 42. Also the zeroth-order moments are determined in this reference.

We consider now the elastic collision region, determined by the reduced energy ϵ [Eq. (22)], in such a way that $\epsilon \lesssim 1$. Here the electronic stopping power $NS_e(E)$ usually is small compared to the nuclear stopping power $NS_t(E)$, unless $Z_1 \lesssim \frac{1}{10}Z_2$. Thus, the electronic stopping powers in the denominator of $\eta_{(p)}$ and $\eta_{(r)}$ can be ignored.

Thus, it is straightforward to evaluate the integrals for the zeroth-order moments in this energy region. Utilizing the power cross section Eq. (18) and the stopping power for a beam ion-target atom interaction with constants C, γ, and m and the electronic stopping power Eq. (26), one obtains

$$\eta_{(p)}(E)=\frac{E}{(\frac{1}{2}+2m)}\frac{NS_e(E)}{NS_t(E)} \quad , \tag{92a}$$

and

$$\eta_{(r)}(E)=\frac{(1-m)}{m}\gamma^{-1}\int_o^{\gamma E}dT\,\frac{\eta_{(l)}(T)}{T} \times\left[\left(\frac{\gamma E}{T}\right)^m-1\right] \quad . \tag{92b}$$

A more precise determination of $\eta_{(r)}(E)$ requires knowledge of the behavior of the energy $\eta_{(l)}(E)$. This energy function is generally well approximated by

$$\eta_{(l)}(E)=k_\omega E^\omega \quad , \tag{93}$$

which leads to a simplification of Eq. (92b):

$$\eta_{(r)}(E)=\frac{(1-m)}{\omega(\omega-m)}\gamma^{-1}\eta_{(l)}(\gamma E) \quad . \tag{94}$$

The power approximation (93) is actually rather accurate for values of the reduced energy ϵ in the interval [0.2,2], and ω varies even less than 10% for all values of the electronic stopping-power constant k_L [Eq. (25)], which are feasible for any target-target combination.

One notices that the amount of energy delivered to the electrons by recoiling target atoms is not directly proportional to $\eta_{(l)}(E)$, but to the scaled energy $\eta_{(l)}(\gamma E)$. This is not surprising as γE is the max-

imum energy transfer in a beam ion-target atom collision.

The equations for $D_{(p)}$ and $D_{(t)}$ can now be solved by means of the same procedure as was utilized in Secs. II and III. Thus, the spatial moments of the two distributions may be determined from a recursive formula analogous to Eqs. (14) or (42). This is possible once the zeroth-order moments of the distributions have been found.

C. Scaling properties of the distributions $D_{(p)}$ and $D_{(r)}$

The important length unit in the energy (and range) distributions for atomic incidence for reduced energies below $\epsilon=1$ is E^{2m}/NC. For example, the path length $R(E)$, obtained by integration of the reciprocal power approximation to the nuclear stopping power $NS_t(E)$, is expressed:

$$R(E)=\frac{(1-m)}{2m}\gamma^{m-1}\left[\frac{E^{2m}}{NC}\right] . \tag{95}$$

This length unit E^{2m}/NC is obviously useful only so long as the electronic stopping power can be neglected. If this can be done, the transport equations for $D_{(p)}$ and $D_{(t)}$ are, apart from the normalization, analogous to the equations treated in Ref. 37. $D_{(p)}$ and $D_{(t)}$ are both given, then, by the following relation:

$$D_{(p)}(x,E,\vec{e})=\eta_{(p)}(E)\frac{NC}{E^{2m}}f_p\left[\frac{xNC}{E^{2m}}\right] . \tag{96}$$

(The equation for $D_{(r)}$ is obtained by replacing the subscript p with r.) The dimensionless functions f_p and f_r can be constructed from the spatial moments of the distributions. Moreover, once all lengths are expressed in the length unit noted above, f_p and f_r become independent of the primary energy (for the same exponent m). These functions depend only on the mass ratio M_2/M_1 and m.

Equation (96) for $D_{(p)}$ is now changed by means of Eq. (92a) to

$$D_{(p)}(x,E,\vec{e})=\frac{(1-m)}{\frac{1}{2}+2m}\gamma^{m-1}NS_e(E)f_p\left[\frac{xNC}{E^{2m}}\right] . \tag{97a}$$

The relation corresponding to Eq. (97a) for the recoil-induced distribution $D_{(r)}$ is obtained by means of Eq. (92b)

$$D_{(r)}(x,E,\vec{e})=\frac{(1-m)^2}{\omega(\omega-m)}\gamma^{m-1}NS_t(E)\times\frac{\eta_{(t)}(\gamma E)}{\gamma E}f_r\left[\frac{xNC}{E^{2m}}\right] , \tag{97b}$$

where ω again is determined from a power approximation (93) to the energy function $\eta_{(t)}(E)$. From Eq. (61) one concludes that for large E the energy dependent factor $NS_t(E)\eta_{(t)}(\gamma E)/(\gamma E)$ will approach the nuclear stopping power $NS_t(E)$.

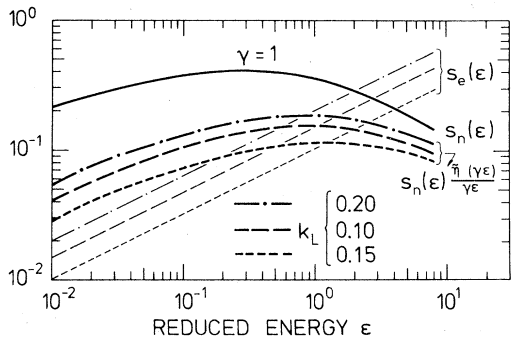

FIG. 12. Factor $s_n(\epsilon)\tilde{n}_{(t)}(\gamma\epsilon)/\gamma\epsilon$, Eq. (98), and the reduced electronic stopping powers $s_e(\epsilon)$, Eq. (25), are depicted as functions of the reduced energy ϵ, Eq. (22), for three values of the constant k_L. (——·——), $k_L=0.20$ (————————), $k_L=0.15$; (– – –), $k_L=0.10$. The reduced nuclear stopping power $s_n(\epsilon)$, Eq. (21), is also included, (——).

The dimensionless factor $s_n(\epsilon)\tilde{n}_{(t)}(\gamma\epsilon)/(\gamma\epsilon)$ is defined from the expression:

$$NS_t(E)\frac{\eta_{(t)}(\gamma E)}{\gamma E}=\frac{NZ_1Z_2 4\pi e^2 aM_1}{M_1+M_2}\times s_n(\epsilon)\frac{\tilde{n}_{(t)}(\gamma\epsilon)}{\gamma\epsilon} . \tag{98}$$

This factor is depicted in Fig. 12 as a function of the reduced energy ϵ for three representative cases of k_L for a target atom-target atom collision and with $\gamma=1$. One notes that a large electronic stopping power for recoils also means large values of the dimensionless factor, given by Eq. (98); but the variation from the middle one ($k_L=0.15$) does not exceed a factor of 1.5. The shapes of the three curves are similar, and they all reach the maximum value around $\epsilon\approx 1$. Also, the respectively reduced electronic stopping powers are indicated, and they turn out to become larger than the factor at around $\epsilon=1$. For values of γ less than 1 the dimensionless factor decreases to a somewhat lower value, because $\tilde{\eta}_{(t)}(\epsilon)$ decreases as the reduced energy ϵ decreases.

D. Spatial moments of $D_{(p)}$ and $D_{(r)}$

The mean values of the distributions $D_{(p)}$ and $D_{(r)}$ are found by the procedure in Ref. 37. Neglecting the electronic stopping power in the denominator of the first-order moment one obtains for the mean

value $\langle x\rangle_p$ of the primary distribution $D_{(p)}$

$$\langle x\rangle_p = 3A^1_{(p)1}\frac{E^{2m}}{NC}\cos\theta \ . \tag{99}$$

The energy-independent coefficient $A^1_{(p)1}$ is evaluated in Ref. 45. This coefficient depends only on the mass ratio M_2/M_1 and on m.

For the recoil-induced distribution we replace the subscript p with r in Eq. (99). The coefficient $A^1_{(r)1}$ is evaluated in Ref. 45. It is shown that this coefficient is energy independent provided that

$$\eta_{(i)}(E)/\eta_{(r)}(E) \approx \text{constant} \ . \tag{100}$$

This relation is fulfilled so long as the same exponent ω in Eq. (93) is applicable for $\eta_{(i)}(E)$ and for $\eta_{(i)}(\gamma E)$; it turns out that even for values of γ somewhat less than 1, Eq. (100) is valid with acceptable accuracy. The same method yields higher spatial moments expressed by energy independent constants A^n_l and powers of the length unit E^{2m}/NC.

The ratio $\langle x\rangle_p/R$ is shown in Fig. 13 as a function of the mass ratio M_2/M_1 for $m=\frac{1}{2}$ and $\frac{1}{3}$. For a fixed exponent m, the ratio $\langle x\rangle_p/R$ is a relatively slowly varying function of M_2/M_1 and one notices that the ratio is almost unchanged for $M_2/M_1 \lesssim 1$. Also the ratio $\sigma_p^2/\langle x\rangle_p^2$—where $\sigma_p = (\langle (x - \langle x\rangle_p)^2\rangle_p)^{1/2}$ is the standard deviation over the distribution $D_{(p)}$—is slowly varying for $M_2/M_1 \lesssim 2$. Furthermore, the skewness

$$\Gamma_{1,p} = \frac{\langle (x-\langle x\rangle_p)^3\rangle_p}{\sigma_p^3} \ , \tag{101}$$

is shown in Fig. 13. For large M_2/M_1 the scattering obviously leads to a decrease in $\langle x\rangle_p/R$ and an increase in $\sigma_p^2/\langle x\rangle_p^2$.

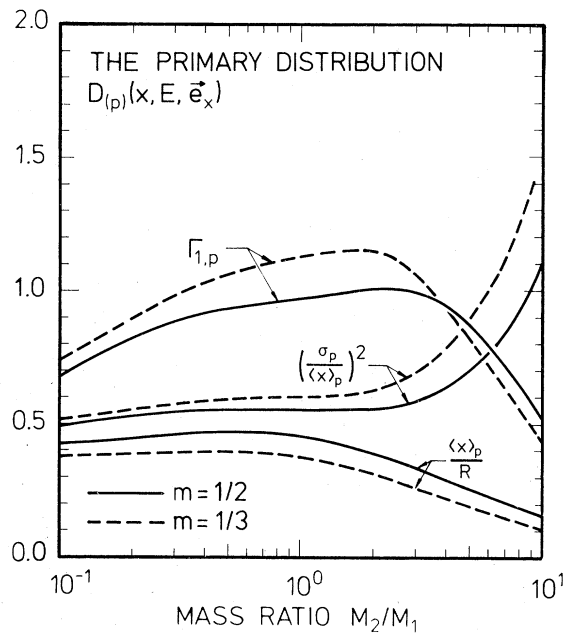

FIG. 13. Characteristic quantities from the primary distribution $D_{(p)}(x,E,\vec{e}_x)$ at perpendicular incidence depicted as a function of the mass ratio M_2/M_1 for two different exponents m in the power cross section. (——), $m=\frac{1}{2}$; (– – –), $m=\frac{1}{3}$. $\langle x\rangle_p$ is the average depth for primary ionization, Eq. (99); R = path length, Eq. (95); $\sigma_p = (\langle (x-\langle x\rangle_p)^2\rangle_p)^{1/2}$; $\Gamma_{1,p}$, the skewness, Eq. (101). The term representing electronic stopping power has been neglected in the total stopping power [Eq. (15a), Ref. 42].

In Fig. 14 the characteristic quantities of the recoil-induced distribution have been depicted as a function of M_2/M_1. The ratio $\langle x\rangle_r/R$ decreases for increasing mass ratio over more than one order of magnitude in M_2/M_1. The source of the decrease is again the scattering of the primaries. Also $\sigma_r^2/\langle x\rangle_r^2$ increases for increasing mass ratio for the same reason.

In Fig. 15 the characteristic recoil-induced quantities have been compared to the corresponding damage distribution quantities for the two exponents $m=\frac{1}{2}$ and $\frac{1}{3}$. One notices that the quantities of the two distributions are almost equal, which means that the distributions have nearly the *same shape*. Of course, the normalization is different.

The characteristic quantities for the total distribution $D_{(b)}$ have been calculated with $m=\frac{1}{2}$ from the corresponding quantities for $D_{(p)}$ and $D_{(r)}$ (Table

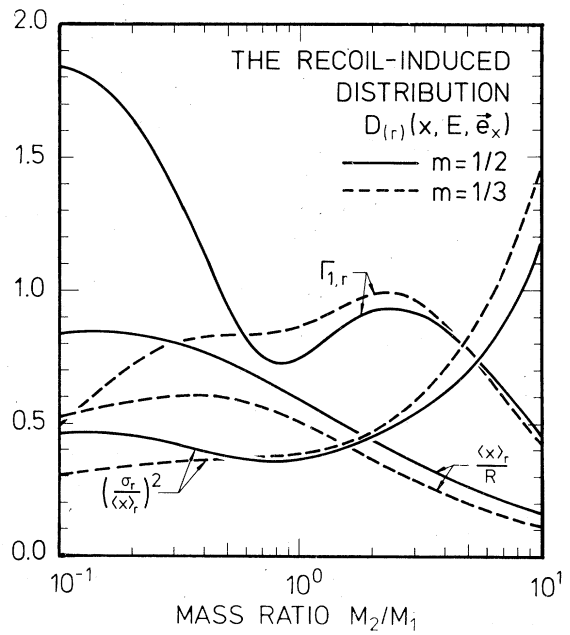

FIG. 14. Characteristic quantities from the recoil-induced distribution $D_{(r)}(x,E,\vec{e}_x)$ at perpendicular incidence. $\langle x\rangle_r$ is the average depth for ionization by recoiling target atoms. Otherwise, notation and comments are as in Fig. 13.

TABLE VI. Comparison between quantities characteristic for the distribution $D_{(b)}(x,E,\vec{e}_x)$ calculated by the procedure indicated in Secs. XII B–XII D and by Winterbon in Refs. 39 and 115. The results from the present work have been obtained with use of Eqs. (91), (92a), (94), with $\omega=1.2$, Eq. (93), and with $m=\frac{1}{2}$; the electronic stopping power has been neglected except in Eq.(92a).

Ion-target combination		Kr→Cu	Xe→Cu
Primary energy (keV)		204	219
Reduced energy ϵ		0.6	0.3
$\eta_{(b)}(E)/E$	This work	0.451	0.374
	Ref. 39	0.396	0.366
$\langle x\rangle_b/R$	This work	0.577	0.659
	Ref. 39	0.508	0.543
$\sigma_b^2/\langle x\rangle_b^2$	This work	0.448	0.459
	Ref. 39	0.420	0.417
$\Gamma_{1,b}$	This work	0.818	1.03
	Ref. 39	0.668	0.740

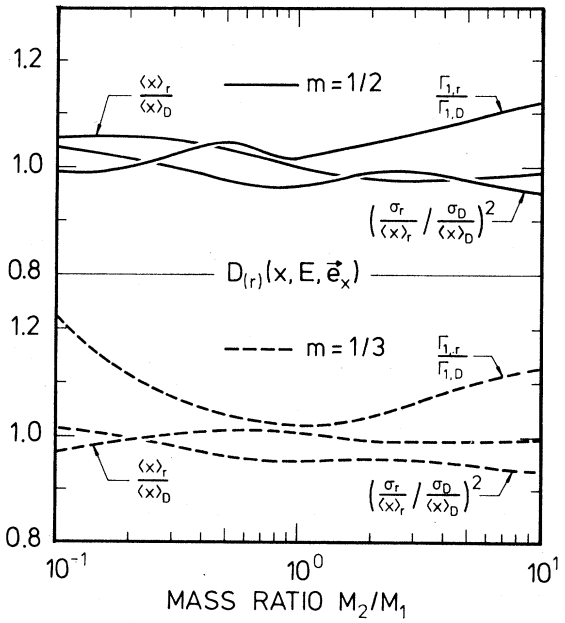

FIG. 15. Ratio of the quantities of the recoil-induced distribution $D_{(r)}(x,E,\vec{e}_x)$ to the corresponding quantities of the damage distribution $D_{(D)}(x,E,\vec{e}_x)$. For notation and comments, see Fig. 14.

VI). The results obtained in this way for the cases mentioned above agree better than 20% in most cases with Winterbon's calculations[39,115] in which electronic stopping is included in all moments of $D_{(b)}$. The skewness deviates somewhat more; however, one notes from Fig. 14 that the skewness of $D_{(r)}$ depends significantly on the exponent m (and thereby on the energy E).

E. Construction of the distributions

As discussed in Refs. 37 and 48 it is difficult in general to construct a good approximation to a distribution from a finite number of moments. A reasonable approximation requires an appropriate assumption of the behavior of the real distribution.

As the spatial energy deposition by the primaries or by the recoiling target atoms must differ according to the nature of the processes induced by the two kinds of particles, the primary distribution $D_{(p)}$ and the recoil-induced distribution $D_{(r)}$ must be constructed on the basis of widely different assumptions. The energy transport by recoiling electrons will, as a first step, be ignored in the constructions; the influence of this transport will be discussed in the following section.

Although general construction methods for the total distribution $D_{(b)}$ are available,[39,48,65] usually a large number of moments are needed for a reliable reconstruction of the distribution. The separation of $D_{(b)}$ into the two distributions, in which each can be

approximated in a feasible way, will be utilized here, as only a few moments will be included.

The distribution $D_{(p)}$ is determined by the scattering of the primaries and their electronic stopping power. It is demonstrated below that $\langle x\rangle_p/R$ in the limit $M_2/M_1=0$ has the value

$$\frac{\langle x\rangle_p}{R}=\frac{4m}{8m+1}\quad (M_2/M_1=0)\ . \tag{102}$$

$M_2/M_1=0$ represents the limiting case of a very heavy primary particle that penetrates a target consisting of light atoms; the primary is undeflected over its whole path length. Because $\langle x\rangle_p/R$ deviates less than only 20% from this limit for mass ratios $M_2/M_1\leq 1$ in the energy regions characterized by the exponents $m=\frac{1}{2}$ and $\frac{1}{3}$, an energy-loss distribution in the limit $M_2/M_1=0$ seems suitable for a construction of the distribution $D_{(p)}$.

Obviously, the energy δE, deposited to the electrons in a layer δx by a primary with the instantaneous energy $E^*(x)$ is determined by the electronic stopping power Eq. (26):

$$\delta E=Nk[E^*(x)]^{1/2}\delta x\ . \tag{103}$$

In the reduced energy region $\epsilon\lesssim 1$ under consideration, the energy dependence on depth for an undeflected (heavy) primary is

$$E^*(x)=E\left[1-\frac{x}{R}\right]^{1/2m}\ . \tag{104}$$

This relationship holds, of course, only when the electronic stopping power can be ignored in the total stopping power. Hence, the primary distribution in the limit $M_2/M_1=0$ for a particle moving perpendicular to the plane $x=0$ becomes

$$D_{(p)}(x,E,\vec{e}_x)=\begin{cases}NS_e(E)(1-x/R)^{1/4m} & \text{for } 0\leq x\leq R\\ 0 & \text{for } x<0 \text{ or } x\geq R\end{cases}\ . \tag{105}$$

This expression will be used, then, for the construction of the primary distribution for all mass ratios less than one. One notes that the distribution Eq. (105) possesses at $x=0$ a discontinuity, because energy transport by recoil electrons has been ignored and also because no backscattering of the primaries takes place in the limit $M_2/M_1=0$.

The moments of the distribution Eq. (105) [and $\langle x\rangle_p/R$ in Eq. (102)] are easily evaluated. These moments can also be evaluated by means of the procedure described in Ref. 45. Because of the statistical nature of the recoil generation, the distribution $D_{(r)}$ is similar to a Gaussian in the energy region $\epsilon\lesssim 1$ considered,[33] and the distribution may, therefore be approximated by Edgeworth's expansion with a few moments.[33,36,37,45] Here the skewness Eq. (101) is included, but not terms originating from moments higher than $n=3$.

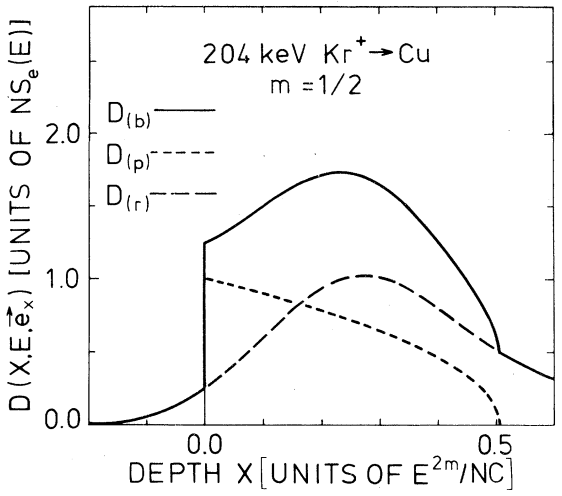

FIG. 16. Total distribution $D_{(b)}(x,E,\vec{e}_x)$, (——); the primary distribution $D_{(p)}(x,E,\vec{e}_x)$, (– – –); and the recoil-induced distribution $D_{(r)}(x,E,\vec{e}_x)$, (—— ——), for normal incidence of 204-keV krypton ions on copper. The distributions are depicted [in units of the stopping power $NS_e(E)$] as a function of the depth x (in units of E^{2m}/NC). An exponent $m=\frac{1}{2}$ in the power cross section has been used. $D_{(p)}$ is constructed by means of Eq. (105), $D_{(r)}$ by means of an Edgeworth expansion, Ref. 33, and $D_{(b)}$ by means of $D_{(b)}=D_{(p)}+D_{(r)}$. The exponent $\omega=1.2$, Eq. (93).

In Figs. 16 and 17 the primary distribution $D_{(p)}$, the recoil-induced distribution $D_{(r)}$, and the total distribution $D_{(b)}=D_{(p)}+D_{(r)}$ are shown for incident krypton and xenon ions on copper perpendicular to the surface with the energy in the range of 200 keV.

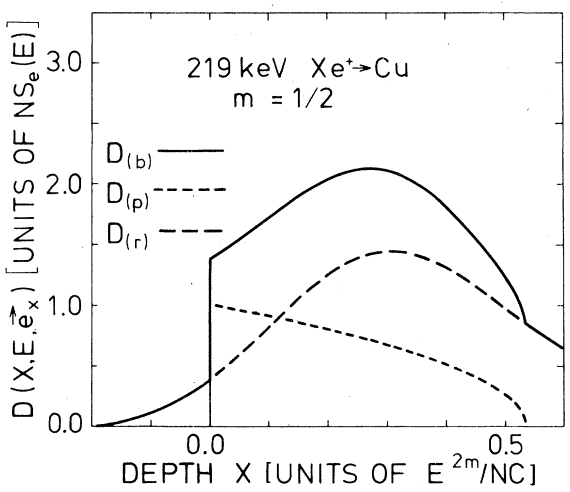

FIG. 17. Distributions $D_{(b)}(x,E,\vec{e}_x)$, $D_{(p)}(x,E,\vec{e}_x)$, and $D_{(r)}(x,E,\vec{e}_x)$ for normal incidence of 219-keV xenon ions on copper. For comments, see Fig. 16.

For a fixed exponent m the shape is energy independent as mentioned, but the zeroth-order moments $\eta_{(p)}$ and $\eta_{(r)}$ depend on the energy. In both cases the energy deposited by the recoils exceeds the energy that is lost directly from the primaries to the electrons. However, the recoil-induced energy is deposited at considerably larger depths, which leads to a smaller surface value for $D_{(r)}$ than for $D_{(p)}$ in this approximation (without recoiling electrons).

F. Yield evaluation

According to the separation of the distribution $D_{(b)}$, the basic yield equation (77) is rewritten in the form

$$\delta = [D_{(p)}(0,E,\vec{e}) + D_{(r)}(0,E,\vec{e})]\Lambda \ , \qquad (106)$$

where Λ is the material parameter Eq. (78), and where the surface value of the total distribution is divided into its two parts. The surface value of the primary distribution is equal to the stopping power $NS_e(E)$ (in the absence of any energy transport by the recoil electrons).

The surface value of the recoil-induced distribution may be expressed by means of the dimensionless function $\beta_r(E,\vec{e})$:

$$\beta_r NS_t(E)\frac{\eta_{(t)}(\gamma E)}{\gamma E} = D_{(r)}(0,E,\vec{e}) \ . \qquad (107)$$

The function β_r depends relatively strongly on the direction $\vec{e}$ and on the mass ratio M_2/M_1, and weakly on the primary energy E. The energy transport by recoiling electrons is neglected here as well. By means of the power cross section and the Edgeworth expansion, β_r is found in Ref. 42.

As m depends only weakly on the primary energy, β_r varies slowly as a function of the primary energy in the region $\epsilon \lesssim 1$. β_r is depicted as a function of the mass ratio for two exponents in Fig. 18. One notes that β_r for $M_2/M_1 \geq 0.5$ does not exhibit a large variation from $m = \frac{1}{3}$ to $\frac{1}{2}$; this again corresponds to a slow energy variation. Furthermore, β_r is almost constant for $M_2/M_1 \leq 1$.

In Sec. XII D it was found that the damage distribution and the recoil-induced distribution are similar in shape. Thus β_r is nearly proportional to the factor α_D, which has been calculated for power cross sections in the elastic collision region by Sigmund[33] or by Winterbon,[39] the last named including the electronic stopping power. The factor α_D has been incorporated into Fig. 18. The similarity of the two distributions leads by means of the power cross section to the following approximate relationship

$$\beta_r = \frac{(1-m)}{\omega(\omega-m)}\alpha_D \ ; \qquad (108)$$

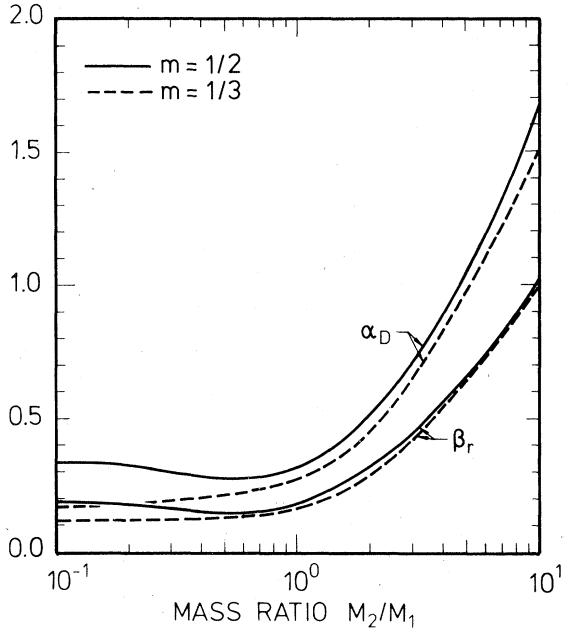

FIG. 18. Factor β_r, Eq. (107), for perpendicular incidence depicted as a function of the mass ratio M_2/M_1 for two exponents m of the power cross section. No correction for energy transport by recoil electrons has been performed. The exponent $\omega = 1.2$, Eq. (93). $f_r(0)$ in Eq. (107) has been determined by an Edgeworth expansion, Refs. 33 and 45. The corresponding factor α_D of the damage distribution $D_{(D)}(x,E,\vec{e}_x)$ has been included for comparison.

this holds better than 12% for mass ratios in the interval $[\frac{1}{10}, 10]$.

The contribution from recoiling electrons has been neglected so far. The correction Eq. (81) for energy transport away from the plane $x = 0$ is comparatively inaccurate in the energy region below the electronic stopping-power maximum, because the correlation between energy transfer and scattering angle is not strictly valid here. The corresponding factor β depends on double differential cross sections for electron ejection (which are usually unknown for the moment) from the primary collision processes. As β_0 depends only weakly on the exponent m for copper, it is tempting to extract with $\beta = \beta_0$ an experimental material parameter for krypton and xenon ions incident on copper by means of Eq. (106); this is similar to the procedure used in Sec. X E. The surface value of the primary distribution is, then, $0.23\,NS_e(E)$. Since the angular distribution of the sputtered particles is forward peaked, the surface value of the recoil-induced distribution is reduced by a factor $1-\beta_0 = 0.77$ as a first approximation. The material parameters obtained are listed in Table V. The corrections for energy transport means that the profiles near the surface in Figs. 16 and 17 are modified. The contributions from recoiling target atoms for

krypton and xenon ions are then, respectively, 0.73 and 1.28 of the contributions directly from the primaries.

In view of the unknown collision spectra the agreement with the proton data and the helium data, which lead to material parameters around 0.26 Å/eV, is satisfactory. In Ref. 42 the parameters, obtained by using the stopping power for the surface value of $D_{(p)}$ and the full surface value of $D_{(r)}$, have been compared; also the parameters, determined in this way, agree in an acceptable manner.

XIII. SUMMARY

A. Results for the secondary electron yield

The secondary electron yield is predicted by Eq. (77) for all kinds of incident particles. For primary *electrons* of nonrelativistic energies above 0.5–1 keV impinging on a solid, the surface value $D_{(e)}(0,E,\vec{\epsilon})$ of the deposited energy can be expressed by means of the factor β and the electronic stopping power $NS_e(E)$. Thus, Eq. (80) can be applied, and β determined from Eq. (84) as well as the data of the references mentioned in Sec. VI A.

For incident *ions* of energies larger than $\frac{1}{2}M_1v_B^2$ (around 25 keV/amu), Eq. (80) can be utilized. The factor β may, in the case of almost no backscattering of the primaries, be set equal to β_0 Eq. (81), which is determined from an appropriate value of the fraction of reflected energy k_pE^{-p} for perpendicular electron incidence. If the factor β_0 is slowly varying as a function of the exponent m in the power cross section (or in the corresponding stopping power) for a beam atom-target electron interaction, formula (80) can be extended to somewhat lower primary energies.

For *ion-target combinations with* $M_2/M_1 \lesssim 1$ with reduced energies ϵ, Eq. (22), below 10 the yield formula (106) is useful. For reduced energies $\epsilon \lesssim 1$, one may as a first step set the surface value $D_{(p)}(0,E,\vec{\epsilon}_x)$ of the primary distribution equal to the electronic stopping power $NS_e(E)$. β_r, Eq. (107), may be determined from Fig. 18 or from Eq. (108) and tabulations of α_D.[39] If β_0, Eq. (81), again is a slowly varying function of the exponent m, the surface value $D_{(p)}(0,E,\vec{\epsilon}_x)$ may be set equal to $\beta_0NS_e(E)$, and the factor β_r may be reduced with an approximate factor $(1-\beta_0)$.

The material parameter Λ in the yield formula (78) can be evaluated if the low-energy electronic stopping power $NS_{e,e}(E_0)$ is available. Otherwise, one may evaluate an extracted experimental parameter from the yield from different beam particles, by dividing with $D(0,E,\vec{\epsilon})$.

B. Results for the distributions of the secondaries

The *energy and angular distribution* or the *total energy distribution* of the secondary electrons emitted in a backward direction may be evaluated by means of Eqs. (65), (68), or (69). The simple formula (65) without a surface barrier can be used only at high secondary electron energies $E_0 >> U_0$, where U_0 is the magnitude of the barrier. The deposited energy at the surface must be determined as described above.

Distributions of secondary electrons induced by transmitted beams may be evaluated from Eqs. (75) and (90). *The most probable energy* and the *half width* $(\Delta E)_{1/2}$ of the energy spectrum are determined by Eq. (72) and from Fig. 5, if m in the low-energy stopping power expression (70) is known. If this stopping power is unknown, the exponent m can be extracted from the experimental spectrum by means of either Eq. (68) or Eq. (69), and the most probable energy and the half width may then be determined for comparison with the experimental spectrum.

C. Feasible comparisons between theory and experiment

Although the treatment has been derived for a semi-infinite medium, the results are applicable to thick *foils* as well, so long as the cascade of recoiling target particles can develop without interruptions by the surfaces. This means for electron and ion bombardment that the foil thickness d should be much larger than the range of the most energetic recoil electrons.

The *primary energy* E should be so large compared with the instantaneous energy E_0 of the liberated electrons that the isotropic approximation (40) holds in a satisfactory way. For electron bombardment the most important correction term to the leading term $(\sim E/E_0)$ is proportional to $(E/E_0)^{s_1}$, with $s_1 < \frac{1}{2}$.[45] For ion bombardment the correction term is of the same order.[45] This means that a comparison between experimental and theoretical spectra is justifiable at most up to an energy E_0 at which the two terms are comparable. In the yield evaluation the correction terms play a minor role because the electron spectrum peaks at low energy.

Even a small amount of *surface impurities* will change the surface barrier and the stopping power $NS_{e,e}(E_0)$ for the low-energy electrons.

With regard to the *angle* of incidence θ one obtains for light ions the yield at normal incidence by multiplying with $\cos\theta$ up to angles around $\theta = 50°$.[114] For electrons[116] and heavy ions[112] the behavior is more complex.

Some discrepancies between theory and experiment will be expected for *low-energy ions* in the region with velocity-proportional stopping power, since a power cross section with the struck electron initially at rest has been utilized in the present work.

ACKNOWLEDGMENTS

The author is indebted to Peter Sigmund for his continual support and valuable criticism, which have made this work possible, and for letting the author make use of his unpublished work, Sputtering II. Discussions with and comments from Nils Andersen, Peter Børgesen, Niels E. Christensen, Wolfgang Hofer, Gillis Holmén, Uffe Littmark, Bengt Svensson, and Hans Sørensen have been appreciated by the author. The author thanks G. Holmén and B. Svensson, D. Combecher and co-workers, L. Toburen and R. G. Musket for the opportunity to use their unpublished data in the present work. Thanks are due Physical Laboratory II, University of Copenhagen, for generously making available its computing facilities.

---

[1]A. J. Dekker, Solid State Phys. 6, 251 (1958).
[2]O. Hachenberg and W. Brauer, Adv. Electron. Electron Phys. 11, 413 (1959).
[3]G. Carter and J. S. Colligon, *Ion Bombardment of Solids,* (Heinemann, London, 1968), p. 38.
[4]K. H. Krebs, Fortschr. Phys. 16, 419 (1968).
[5]G. M. McCracken, Rep. Prog. Phys. 38, 241 (1975).
[6]C. E. Kuyatt, in *Methods of Experimental Physics,* edited by B. Bederson and W. L. Fite (Academic, New York 1968), Vol. 7A, p. 1.
[7]S. Matteson and M.-A. Nicolet, Nucl. Instrum. Methods 160, 301 (1979).
[8]*Proceedings of an Advisory Group Meeting on Atomic and Molecular Data for Fusion, Culham, 1976* (International Atomic Energy Agency, Vienna, 1977), p. 55.
[9]F. L. Vook, H. K. Birnbaum, T. H. Blewitt, W. L. Brown, J. W. Corbett, J. H. Crawford, Jr., A. N. Goland, G. L. Kulcinski, M. T. Robinson, D. N. Seidman, F. W. Young, Jr., J. Bardeen, R. W. Balluffi, J. S. Koehler, and G. H. Vineyard, Rev. Mod. Phys. 47, Suppl. No. 3, S1 (1975).
[10]H. Vernickel, Phys. Rep. 37, 93 (1978).
[11]L. W. Hobbs, in *Specialists Periodical Reports, Advances of Surface and Defect Properties of Solids,* edited by M. W. Roberts and J. M. Thomas (Chemical Society, London, 1976), Vol. 4, p. 152.
[12]H. Ibach, in *Electron Spectroscopy for Surface Analysis,* edited by H. Ibach (Springer, Berlin, 1977), p. 1.
[13]P. A. Wolff, Phys. Rev. 95, 56 (1954).
[14]E. J. Sternglass, Phys. Rev. 108, 1 (1957).
[15]H. Seiler, Z. Angew. Phys. 22, 249 (1967).
[16]Niels Bohr, Mat. Fys. Medd. Dan. Vid. Selsk. 18, No. 8 (1948).
[17]H. D. Hagstrum, Phys. Rev. 96, 336 (1954).
[18]L. M. Kishinevsky, Radiat. Eff. 19, 23 (1973).
[19]U. A. Arifov, *Interaction of Atomic Particles with a Solid Surface* (Plenum, New York, 1969).
[20]I. M. Bronshtein and B. S. Fraiman, *Secondary Electron Emission* (in Russian) (Nauka, Moscow, 1969).
[21]E. M. Baroody, Phys. Rev. 78, 780 (1950).
[22]H. Stolz, Ann. Phys. 3, 197 (1959).
[23]G. F. Amelio, J. Vac. Sci. Techn. 7, 593 (1970).
[24]E. S. Parilis and L. M. Kishinevsky, Sov. Phys. Solid State 3, 885 (1960) [Fiz. Tverd. Tela 3, 1219 (1960)].
[25]L. M. Kishinevsky and E. S. Parilis, Bull. Acad. Sci. USSR, Phys. Ser. 26, 1432 (1962) [Izv. Ak. Navk. SSSR, Ser. Fiz. 26, 1409 (1962)].
[26]L. N. Dobretsov, Bull. Acad. Sci. USSR, Phys. Ser. 20, 899 (1956) [Izv. Ak. Navk. SSSR, Ser. Fiz. 20, 994(1956)].
[27]H. Bruining, *Physics and Applications of Secondary Electron Emission* (Pergamon, London, 1954), p. 78.
[28]H. Kanter, Phys. Rev. 121, 677 (1961).
[29]K. Kanaya and S. Ono, Jpn. J. Appl. Phys. 13, 944 (1974).
[30]K. Kanaya and H. Kawakatsu, J. Phys. D 5, 1727 (1972).
[31]R. G. Musket, J. Vac. Sci. Techn. 12, 444 (1975).
[32]A. Koyama, E. Yagi, and H. Sakairi, Jpn. J. Appl. Phys. 15, 1811 (1976).
[33]P. Sigmund, Phys. Rev. 184, 383 (1969).
[34]H. H. Andersen, in *Physics of Ionized Gases, 1974,* edited by V. Vujnović (Institute of Physics, Zagreb, Yugoslavia, 1974), p. 361.
[35]J. Lindhard, V. Nielsen, M. Scharff, and P. V. Thomsen, Mat. Fys. Medd. Dan. Vid. Selsk. 33, No. 10 (1963).
[36]J. B. Sanders, thesis (University of Leiden, 1968) (unpublished).
[37]K. B. Winterbon, P. Sigmund, and J. B. Sanders, Mat. Fys. Medd. Dan. Vid. Selsk. 37, No. 14 (1970).
[38]D. K. Brice, in *Ion Implantation Range and Energy Distributions,* edited by D. K. Brice (Plenum, New York, 1975), Vol. 1.
[39]K. B. Winterbon, in *Ion Implantation Range and Energy Distributions,* edited by D. K. Brice (Plenum, New York, 1975), Vol. 2.
[40]P. Sigmund, Rev. Roum. Phys. 17, 1079 (1972).
[41]J. Schou, Nucl. Instrum. Methods 170, 317 (1980).
[42]G. Holmén, B. Svensson, J. Schou, and P. Sigmund, Phys. Rev. B 20, 2247 (1979).
[43]H. J. Klein, Z. Phys. 188, 78 (1965).
[44]H. Jahrreiss and W. Oppel, J. Vac. Sci. Techn. 9, 173 (1972).
[45]J. Schou, Risø Report No. M-2218 (1980) (unpublished).
[46]P. Sigmund, Sputtering II (unpublished).
[47]L. I. Schiff, *Quantum Mechanics,* 3rd ed. (McGraw-Hill, New York, 1968), pp. 79–81.
[48]U. Littmark, thesis (University of Copenhagen, 1974) (unpublished).
[49]L. D. Landau and E. M. Lifshitz, *Mechanics,* 3rd ed. (Pergamon, New York, 1976), pp. 44–47.
[50]J. Lindhard, V. Nielsen, and M. Scharff, Mat. Fys. Medd. Dan. Vid. Selsk. 36, No. 10 (1968).
[51]P. Sigmund, Rev. Roum. Phys. 17, 823 (1972).
[52]K. Kanaya and S. Okayama, J. Phys. D 5, 43 (1972).
[53]J. C. Ashley, C. J. Tung, and R. H. Ritchie, Surf. Sci. 81, 409 (1979).
[54]J. Lindhard and M. Scharff, Phys. Rev. 124, 128 (1961).
[55]P. Sigmund, Rev. Roum. Phys. 17, 969 (1972).
[56]R. Weissmann and P. Sigmund, Radiat. Eff. 19, 7 (1973).
[57]H. E. Schiøtt, Mat. Fys. Medd. Dan. Vid. Selsk. 35, No. 9 (1966).
[58]M. T. Robinson, Philos. Mag. 12, 741 (1965).
[59]P. Sigmund, Radiat. Eff. 1, 15 (1969).

[60]A. E. Grün, Z. Naturforsch. Teil A 12, 89 (1957).
[61]A. Cohn and G. Caledonia, J. Appl. Phys. 41, 3767 (1970).
[62]J. L. Barrett and P. B. Hays, J. Chem. Phys. 64, 743 (1976).
[63]T. E. Everhart and P. H. Hoff, J. Appl. Phys. 42, 5837 (1971).
[64]L. V. Spencer, Nat. Bur. Stand. Monogr. 1, 1 (1959).
[65]L. V. Spencer, Phys. Rev. 98, 1597 (1955).
[66]S. K. Gupta and M. A. Prasad, Radiat. Res. 76, 1 (1978).
[67]M. J. Berger, S. M. Seltzer, and K. Maeda, J. Atmos. Terr. Phys. 32, 1015 (1970).
[68]B. Grosswendt and E. Waibel, Nucl. Instrum. Methods 155, 145 (1978).
[69]R. Shimizu, M. Honji, and K. Murata, Jpn. J. Appl. Phys. 9, 1291 (1970).
[70]T. Matsukawa, K. Murata, and R. Shimizu, Phys. Status Solidi B 55, 371 (1973).
[71]H. Paretzke, in *Proceedings of the 4th Symposium on Microdosimetry, Verbania Pallanza, Italy, Sept. 1973,* edited by J. Booz, H. G. Ebert, R. Eickel, and A. Waker (Commission of the European Communities, Luxembourg, 1974), p. 141.
[72]U. Littmark and G. Maderlechner, in *Proceedings of the 8th Yugoslav Symposium on the Physics of Ionized Gases, Dubrovnik, 1976,* edited by B. Navinsek (University of Ljubljana, Ljubljana, 1976), p. 139.
[73]P. Sigmund, in *Proceedings of the 3rd International Conference on Atomic Collisions in Solids, Oct. 1974, Kiev, USSR* (Pbl. No. 74-07, Phys. Lab. II, University of Copenhagen, Copenhagen, 1974).
[74]R. F. Willis and N. E. Christensen, Phys. Rev. B 18, 5140 (1978).
[75]W. B. Nottingham, in *Handbuch Der Physik,* edited by S. Flügge (Springer, Berlin, 1956), vol. 21, p. 1.
[76]M. W. Thompson, Philos. Mag. 18, 377 (1968).
[77]*CRC Handbook of Chemistry and Physics, West Palm Beach,* edited by R. C. Weast (CRC, West Palm Beach, Florida, 1978), p. E-81, or earlier editions.
[78]H. B. Michaelson, J. Appl. Phys. 48, 4729 (1977).
[79]C. J. Tung, J. C. Ashley, and R. H. Ritchie, Surf. Sci. 81, 427 (1979).
[80]C. J. Tung, R. H. Ritchie, J. C. Ashley, and V. E. Anderson, Oak Ridge National Laboratory Report No. ORNL-TM-5188, 1976.
[81]L. R. Peterson and A. E. S. Green, J. Phys. B 1, 1131 (1968).
[82]G. Wehner, Z. Phys. 193, 439 (1966).
[83]T. E. Everhart, N. Saeki, R. Shimizu, and T. Koshikawa, J. Appl. Phys. 47, 2941 (1976).
[84]D. Roptin, thesis (University of Nantes, 1975) (unpublished).
[85]T. Koshikawa and R. Shimizu, J. Phys. D 6, 1369 (1973).
[86]J. Schaefer and J. Hölz, Thin Solid Films 13, 81 (1972).
[87]F. Louchet, L. Viel, C. Benazeth, B. Fagot, and N. Colombie, Radiat. Eff. 14, 123 (1972).
[88]N. J. Miller, I. Lindau, and W. E. Spicer, in *Proceedings of the International Conference on Transition Metals, Aug. 1977, Toronto,* edited by M. J. G. Lee, J. M. Perz, and E. Fawcett, Inst. Phys. Conf. Ser. No. 39 (IOP, Bristol and London, 1978), p. 244.
[89]R. Bindi, M. Lanteri, and P. Rostaing, J. Electron Spectros. Relat. Phenom. 17, 249 (1979).
[90]D. Combecher, J. Kollerbaur, G. Leuthold, H. G. Paretzke, and G. Burger, in *Proceedings of the 6th Symposium on Microdosimetry, Brussels, May 1978,* edited by J. Booz and H. G. Ebert (Harwood, London, 1978), p. 295.
[91]A. P. Cracknell, *The Fermi Surfaces of Metals* (Taylor and Francis Ltd., London, 1971), p. 75.
[92]L. H. Toburen (private communication).
[93]H. H. Andersen and J. F. Ziegler, *Hydrogen Stopping Powers and Ranges in All Elements* (Pergamon, New York, 1977).
[94]H. Sørensen and J. Schou, J. Appl. Phys. 49, 5311 (1978).
[95]Toburen points out that his foil thickness is somewhat uncertain, and that an increased thickness could lower the intensity by as much as a factor of 2.
[96]Nils Andersen and P. Sigmund, Mat. Fys. Medd. Dan. Vid. Selsk. 39, No. 3 (1974).
[97]R. A. Baragiola, E. V. Alonso, and A. Oliva Florio, Phys. Rev. B 19, 121 (1979).
[98]G. Holmén, B. Svensson, and A. Burén, GIPR-184 (unpublished).
[99]K. -O. Groeneveld, in *Beam-Foil Spectroscopy,* edited by I. A. Sellin and D. J. Pegg (Plenum, New York, 1976), Vol. 2, p. 593.
[100]I. M. Bronshtein and V. M. Stozharov, Sov. Phys. Solid State 12, 2280 (1971) [Fiz. Tverd. Tela 12, 2824 (1970)].
[101]W. E. Wilson and L. H. Toburen, Phys. Rev. A 11, 1303 (1975).
[102]M. J. Berger, S. M. Seltzer, and K. Maeda, J. Atmos. Terr. Phys. 36, 591 (1974).
[103]S. Thomas and E. B. Pattinson, J. Phys. D 3, 349 (1970).
[104]I. M. Bronshtein and B. S. Fraiman, Sov. Phys. Solid State 3, 1188 (1961) [Fiz. Tverd. Tela 3, 1638 (1961)].
[105]G. Holmén and B. Svensson (private communication).
[106]J. Lindhard and A. Winther, Mat. Fys. Medd. Dan. Vid. Selsk. 34, No. 4 (1964).
[107]M. S. Chung and T. E. Everhart, Phys. Rev. B 15, 4699 (1977).
[108]J. P. Ganachaud and M. Cailler, Surf. Sci. 83, 519 (1979).
[109]I. M. Bronshtein and B. S. Fraiman, Radio Eng. Electron Phys. 7, 1530 (1962) [Radiotekn. i Elektron. 7, 1643 (1962)].
[110]R. A. Baragiola, E. V. Alonso, J. Ferron, and A. Oliva Florio, Surf. Sci. 90, 240 (1979).
[111]O. B. Firsov, Sov. Phys. JETP 36, 1076 (1959) [J. Exp. Th. Phys. 36, 1517 (1959)].
[112]Ya. A. Vinokurov, L. M. Kishinevsky, and E. S. Parilis, Bull. Acad. Sci. USSR, Phys. Ser. 40, 166 (1976) [Izv. Akad. Nauk. SSSR, Ser. Fiz. 40, 1745 (1976)].
[113]A. A. Dorozkin, A. N. Miskin, and N. N. Petrov, Bull. Acad. Sci. USSR, Phys. Ser. 38, 60 (1974) [Izv. Nauk SSSR, Ser. Fiz. 38, 249 (1974)].
[114]B. Svensson and G. Holmén (unpublished).
[115]K. B. Winterbon, Chalk River Report No. AECL-3194, 1968, (unpublished).
[116]I. M. Bronshtein and S. S. Denisov, Sov. Phys. Solid State 7, 1484 (1965) [Fiz. Tverd. Tela 7, 1846 (1965)].